Atlantic Technological University Donegal

Department of Electronic and Mechanical Engineering

Underwater Optical Wireless Communication (UOWC)

Final Year Project Report

by

Emil Beauseigneur

L00196279

A report submitted in partial fulfilment of the requirements for a

B.Eng (Honours) Electronic Engineering (Embedded Systems Design)

Supervised by: Mr Martin Bradley

Date: 28 April 2026

Declaration

I declare that this report is entirely my own work and that it has not been submitted for any other award. Where the work of others has been used, it has been acknowledged appropriately through citation and referencing. I understand that plagiarism and other forms of academic misconduct are subject to disciplinary procedures.

Student Name: Emil Beauseigneur

Student Signature: _____

Date: 28 April 2026

Abstract

Underwater communication is fundamental to ocean science, environmental monitoring and the operation of autonomous underwater vehicles. Acoustic links provide long range but are constrained by low data rates, high latency and significant multipath effects, while radio frequency propagation in seawater is severely attenuated. Underwater Optical Wireless Communication (UOWC) provides an attractive short range alternative by exploiting the blue green transmission window of water and using intensity modulation with direct detection to deliver higher data rates with low latency.

This project designs, constructs and evaluates a low cost UOWC prototype using visible LEDs, a silicon photodiode receiver, a transimpedance amplifier, comparator based threshold detection and PSoC embedded hardware. The transmitter was developed around blue, royal blue and green LED sources, while the receiver used a photodiode analogue front end followed by a programmable IDAC and comparator threshold method. The work progressed from initial direct UART bench tests to a more robust comparator based receiver, a mechanically aligned PVC pipe test rig, waterproof enclosures, and field tests using tap water, harbour water and coastal seawater.

The final testing showed that direct UART decoding required near logic level saturation and was therefore unsuitable for weaker optical signals. The IDAC comparator method significantly improved receiver sensitivity by converting smaller analogue pulses into full swing logic transitions. Removing a redundant smoothing capacitor improved the receiver bandwidth, while later tests identified the TPS92612 LED driver as the main data rate bottleneck, with 9600 baud reliable and 19 200 baud close to the practical limit. Underwater communication was ultimately achieved after increasing LED drive current, improving the power supply, reducing baud rate, and accounting for reflections and intersymbol interference within the pipe. Wavelength comparison tests showed stronger performance for royal blue and blue than green in the tested harbour and Ballybunion coastal water samples, suggesting that the coastal water used was relatively clear and closer to a low attenuation blue water condition than initially expected.

Acknowledgements

I would like to thank my supervisor Dr Martin Bradley for guidance and feedback throughout this project, and the ATU Donegal Electronic and Mechanical Engineering staff for access to facilities and equipment. I also acknowledge classmates and peers who provided informal discussion and support during development and debugging.

Contents

List of Figures

List of Tables

Nomenclature / Symbols / Abbreviations

Symbol / Abbreviation	Meaning
UOWC	Underwater Optical Wireless Communication
IM/DD	Intensity Modulation / Direct Detection
OOK	On/Off Keying
PPM	Pulse Position Modulation
PWM	Pulse Width Modulation
APD	Avalanche Photodiode
PIN	PIN Photodiode
TIA	Transimpedance Amplifier
SNR	Signal to Noise Ratio
BER	Bit Error Rate
AUV	Autonomous Underwater Vehicle
ROV	Remotely Operated Vehicle
IoUT	Internet of Underwater Things
IDAC	Current output digital to analogue converter
ISI	Intersymbol Interference
FOV	Field of View
I_0	Initial optical intensity
$I(d)$	Optical intensity after distance d
$c(\lambda)$	Attenuation coefficient as a function of wavelength
$a(\lambda)$	Absorption coefficient
$b(\lambda)$	Scattering coefficient

Table 1: Nomenclature, symbols, and abbreviations used in the report.

1 Introduction

Underwater communication is required for a wide range of marine, environmental, industrial, and research applications, including oceanographic data collection, environmental monitoring, subsea inspection, defence systems, and the coordination of autonomous underwater vehicles (AUVs). Traditional underwater communication systems are normally based on acoustic transmission because sound can travel over long distances in water. However, acoustic links are limited by low data rates, high latency, and susceptibility to multipath propagation. Radio frequency (RF) communication is also unsuitable for most underwater applications because RF signals are rapidly attenuated in conductive seawater due to its high ionic content. These limitations create a need for alternative communication methods where short range, low latency, and higher bandwidth underwater data transfer is required.

Underwater Optical Wireless Communication (UOWC) has emerged as a promising solution for short range underwater links. UOWC uses visible or near visible light to transmit information through water, typically using intensity modulation and direct detection. The most useful wavelengths are generally found within the blue green optical window, approximately 450–550 nm, where seawater attenuation is lower than in the red or infrared regions. This allows optical links to achieve data rates far higher than acoustic systems, while also providing much lower latency. However, UOWC is strongly affected by absorption, scattering, turbulence, water clarity, optical alignment, and ambient background light. As a result, the performance of a practical UOWC system depends not only on the selected wavelength, but also on the transmitter power, receiver sensitivity, filtering, threshold detection, and mechanical alignment of the optical path.

The growing interest in the Internet of Underwater Things (IoUT) further supports the need for compact, low-cost, and energy-efficient underwater communication systems. Future underwater sensor networks, diver communication systems, remotely operated vehicles, and autonomous platforms may require short range high speed links for transferring sensor data, images, commands, or diagnostic information. Within this context, UOWC bridges the gap between long range low bandwidth acoustic systems and extremely short range RF links. It is particularly suitable for applications where the transmitter and receiver are within line of sight or where a controlled optical path can be maintained.

This final year project focuses on the design, construction, and evaluation of a low cost short range UOWC prototype using commercially available LEDs,

a photodiode receiver, analogue signal conditioning, and PSoC based embedded control. The transmitter uses blue, royal blue, and green LEDs to compare wavelength performance in water, while the receiver uses a photodiode, transimpedance amplifier, programmable comparator threshold, and UART based data recovery. A key part of the design is the use of the PSoC IDAC to generate an adjustable comparator baseline, allowing weak analogue optical signals to be converted into full swing digital logic signals once they rise above the selected noise floor.

The project progressed from initial bench testing to a fully constructed waterproof test assembly. Early testing showed that direct UART reception only worked over very short distances because the received optical pulses had to fully saturate the photodiode amplifier output before the UART receiver could decode them correctly. This limitation led to the development of the comparator and IDAC threshold method, which significantly improved signal detection by separating analogue signal sensitivity from digital logic level requirements. Further improvements were made by removing a redundant smoothing capacitor from the receiver path, identifying the LED driver as the main speed bottleneck, improving the power supply arrangement, increasing LED drive current, and constructing a controlled PVC pipe enclosure for underwater testing.

The final system was tested in tap water, harbour water, and coastal water. The project successfully demonstrated underwater optical communication using the developed prototype and provided practical wavelength comparison results. In harbour water, the royal blue LED performed better than the green LED using the IDAC threshold method. In coastal water, all wavelengths performed better than in harbour water, with blue and royal blue outperforming green. These results suggest that the tested Ballybunion coastal water was relatively clear, with the royal blue wavelength showing the strongest received signal margin during the final comparison tests.

This report presents the completed development of the UOWC system, including the background theory, literature review, hardware and firmware design, simulation work, mechanical construction, testing methodology, experimental results, discussion, limitations, and future improvements. The final outcome is not a fully optimised underwater modem, but a working engineering prototype that demonstrates the main principles of underwater optical communication and provides a strong foundation for further development.

1.1 Aim and Objectives

The aim of this project was to design, build, and evaluate a short range underwater optical wireless communication system using visible LEDs as transmitters and a photodiode based receiver. The system was developed as a practical low cost prototype capable of transmitting digital data through water while allowing the effects of wavelength, receiver thresholding, alignment, and water quality to be investigated.

The main objectives of the project were:

- To review existing underwater communication methods and identify where UOWC provides an advantage over acoustic and RF links.
- To investigate the blue green optical transmission window and select suitable LED wavelengths for practical underwater testing.
- To design and build a transmitter based on visible LEDs and a constant current LED driver.
- To develop a receiver using a photodiode, transimpedance amplifier, comparator thresholding, and PSoC embedded hardware.
- To use the PSoC IDAC as an adjustable comparator reference so that weak analogue optical pulses could be converted into reliable digital logic transitions.
- To construct a mechanically aligned and water resistant test assembly for underwater optical communication trials.
- To compare the performance of royal blue, blue, and green LEDs in different water samples.
- To identify the main practical limitations of the system, including optical power, receiver sensitivity, baud rate, reflections, waterproofing, and mechanical robustness.

1.2 Design Brief

The final system was designed to meet the following practical requirements:

- Operate within the 450–550 nm blue green wavelength region, where water attenuation is generally lower.
- Use low cost and laboratory safe LEDs rather than lasers.

- Use a silicon photodiode receiver with analogue signal conditioning and comparator based threshold detection.
- Demonstrate digital data transmission through water using a PSoC based embedded transmitter and receiver.
- Provide a repeatable test platform for comparing wavelength performance and receiver threshold margin.
- Remain mechanically practical for field handling, water filling, LED replacement, and serial data logging.

1.3 Research Questions and Success Criteria

This project was guided by three main research questions. These questions were used to direct the hardware design, firmware development, simulation work, and practical testing of the underwater optical communication link.

RQ1: What range and data rate are practically achievable using a low cost blue green LED for an underwater optical link in controlled and real water test conditions?

RQ2: What receiver architecture provides the best balance between sensitivity, cost, speed, and robustness to ambient light for a short range UOWC prototype?

RQ3: How can weak analogue optical signals be converted into reliable digital data using embedded hardware, comparator thresholding, and UART based communication?

The success of the project was evaluated using both technical and practical criteria. The main technical success criterion was the achievement of a working underwater optical communication link capable of transmitting digital data through water using visible LEDs and a photodiode receiver. Additional success criteria included demonstrating improved detection range compared with direct UART reception, comparing the performance of different LED wavelengths, identifying the main speed and sensitivity limitations of the system, and developing a repeatable testing method using the IDAC controlled comparator threshold.

The project was considered successful because a functional UOWC prototype was designed, built, and tested. The system progressed from short range

bench testing to successful underwater communication in a sealed test assembly. The receiver design was improved through the use of a programmable comparator threshold, and wavelength comparison tests were completed in harbour and coastal water. The final results provide useful evidence for evaluating royal blue, blue, and green LEDs under practical test conditions, while also identifying clear areas for future improvement.

1.4 Scope and Limitations

Several limitations affected the final system. The transmitter output was restricted by the selected LED driver, available supply voltage, thermal considerations, and the need to keep the system safe for laboratory and field testing. The receiver was limited by the sensitivity of the photodiode and amplifier stage, as well as by the available PSoC analogue hardware. Although the IDAC controlled comparator improved weak signal detection, the system still required careful threshold adjustment and alignment.

The test enclosure improved repeatability by creating a fixed optical path, but it also introduced practical issues. Internal reflections inside the PVC pipe may have contributed to intersymbol interference at higher baud rates, making the communication link more reliable at lower data rates. Mechanical limitations were also present, including sealing difficulties, transport damage, and the need for additional support structures during beach testing.

The simulation work used the Beer Lambert attenuation model as a simplified representation of underwater optical loss. This was useful for estimating trends and comparing water types, but it did not fully model scattering, bubbles, turbulence, receiver field of view, reflections, or changing ambient light conditions. Therefore, the model should be treated as an early engineering approximation rather than a complete description of the underwater channel.

Despite these limitations, the project successfully demonstrated underwater optical communication and produced practical results that can guide future improvements in optical alignment, waterproofing, receiver sensitivity, power delivery, and wavelength selection.

1.5 Contributions

The main contributions of this project are:

- A working low cost UOWC prototype using visible LEDs, a photodiode receiver, comparator based threshold detection, and PSoC embedded hardware.

- A practical transmitter design using the TPS92612 LED driver and selected royal blue, blue, and green LUXEON 3535L LEDs.
- A receiver decision method using the PSoC IDAC and comparator to convert weak analogue optical pulses into full swing digital signals.
- A mechanically aligned PVC pipe test rig with waterproofed transmitter and receiver enclosures for repeatable underwater testing.
- Practical wavelength comparison results for harbour and Ballybunion coastal water samples.
- Identification of key system limitations, including LED driver switching speed, receiver bandwidth, internal reflections, threshold sensitivity, and mechanical sealing.
- A Python simulation framework for modelling received optical power, attenuation, SNR, and BER across different water types and hardware parameters.

1.6 Report Structure

Chapter 2 introduces the background theory of underwater optical communication, including absorption, scattering, the blue green optical window, link budget considerations, IM/DD modulation, and receiver noise. Chapter 3 reviews relevant literature and connects previous UOWC research to the design choices made in this project. Chapter 4 defines the system requirements and specification. Chapter 5 presents the system design, including the transmitter, receiver, modulation method, firmware approach, and component selection. Chapter 6 describes the simulation and modelling work. Chapter 7 documents early implementation and debugging, including receiver sampling and UART synchronisation issues. Chapter 8 describes the experimental methodology used to test the prototype. Chapter 9 presents the practical development work, field testing, and final results. Chapter 10 discusses project management, risk, safety, and sustainability. Chapter 11 evaluates the final system and discusses future development. Chapter 12 concludes the report.

2 Background and Theory

2.1 Underwater Optical Channel: Absorption and Scattering

Water strongly shapes optical propagation through absorption and scattering. Absorption converts optical energy into heat, while scattering redistributes light and reduces the amount of energy that remains within the receiver's field of view. Both effects vary with wavelength and with water composition, including pure water, coastal water, and turbid harbour water. A key practical consequence is the blue green window: in many natural waters, attenuation is minimised roughly in the 450–550 nm range, motivating the use of blue and green sources for UOWC (Pope and Fry, 1997; Kaushal and Kaddoum, 2016). For engineering design, the combined effect is captured by the beam attenuation coefficient $c(\lambda) = a(\lambda) + b(\lambda)$, where a is absorption and b is scattering. Figure 2.1 and Figure 2.2 illustrate typical wavelength dependence and highlight why optical wavelength choice is a first order design decision.

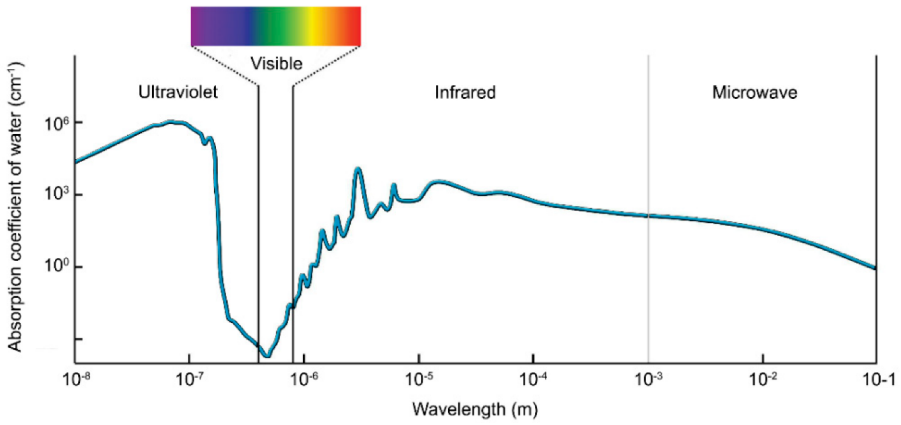

Figure 2.1: Absorption at different wavelengths.

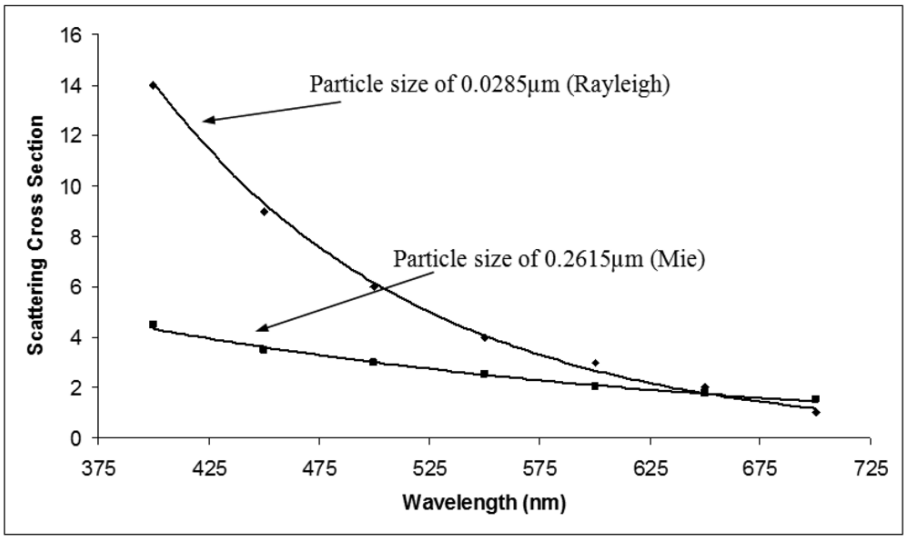

Figure 2.2: Scattering versus wavelength.

2.2 Link Budget Considerations

A link budget for an LED based UOWC system combines transmitted optical power, geometric spreading and optical coupling, water attenuation, receiver responsivity, and front end gain. A convenient starting point is Beer Lambert attenuation with a lumped coupling term, giving the received optical power as:

$$P_r = P_t \eta_{tx} \eta_{rx} G_{geo}(d) e^{-c(\lambda)d} \tag{2.1}$$

where P_t is transmitted optical power, $c(\lambda)$ is the attenuation coefficient, d is range, $G_{geo}(d)$ captures geometric spreading and collection due to divergence and finite receiver aperture, and η_{tx} and η_{rx} capture optical efficiencies such as lens loss, window loss, filter transmission, and alignment or field of view coupling. In practice, receiver side terms can dominate at short ranges because aperture size, lens choice, and alignment determine how much of the diverging LED emission is actually collected.

Once P_r is estimated, the expected photodiode current is:

$$I_p = R(\lambda) P_r \tag{2.2}$$

where $R(\lambda)$ is photodiode responsivity. This current is converted to a voltage using a transimpedance amplifier or equivalent front end and compared against noise and decision thresholds to judge whether reliable decoding is feasible (Schirripa Spagnolo, Cozzella and Leccese, 2020).

2.3 Intensity Modulation and Direct Detection

Most practical UOWC prototypes use intensity modulation and direct detection (IM/DD): the transmitted information is embedded in optical intensity, and the receiver measures intensity through a photodiode without coherent phase recovery. IM/DD simplifies hardware and is compatible with LEDs, but it requires careful management of ambient light and receiver electrical bandwidth. Higher bandwidth supports higher symbol rates but increases integrated noise, reducing the available SNR unless received optical power is increased. Ambient light is not a small detail underwater. Sunlight at the surface, tank lighting, and reflections produce a DC photocurrent that can saturate the front end amplifier. Engineering mitigations include optical bandpass filters matched to the LED wavelength, physical shielding, limiting the receiver field of view, and high pass or AC coupling in the analogue chain.

2.3.1 OOK and PPM

On Off Keying (OOK) is the simplest IM/DD scheme: bits are mapped to light OFF or ON. Pulse Position Modulation (PPM) encodes information in the position of a narrow pulse within a symbol frame. PPM is attractive in optical channels because it concentrates energy into short pulses, which can improve detectability at low average optical power, but it requires more precise timing at the receiver. Figure 2.3 illustrates the difference between pulse width modulation and pulse position modulation, highlighting that PPM detection is a timing problem as much as an amplitude problem.

A key lesson from firmware debugging was that sampling and decoding must be synchronised to the transmitter symbol structure. When receiver sampling is not aligned to symbol boundaries, a single transmitted high can be detected multiple times, or missed, depending on sampling phase. This creates the illusion of extra bits. This is a synchronisation and framing issue and is discussed further in Chapter 7.

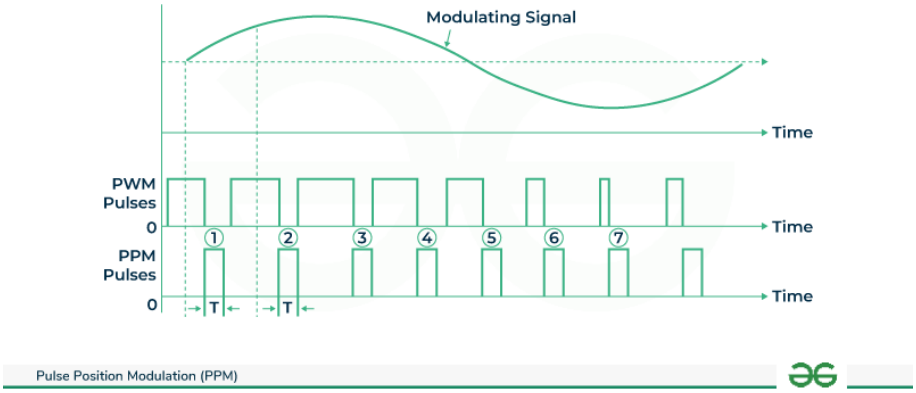

Figure 2.3: Illustrative comparison of PWM and PPM concepts.

2.4 Noise Sources and Receiver Bandwidth

In a photodiode receiver, the dominant noise mechanisms depend on optical power level and front end design. Shot noise arises from the quantised nature of photocurrent and scales with the square root of current, while thermal noise is set by amplifier and resistor noise densities. Ambient light increases DC photocurrent and therefore shot noise, even if the desired signal is small. This is why optical filtering and limiting the field of view can provide a double benefit: they reduce both saturation risk and noise. Receiver bandwidth B also affects noise power because integrated noise grows with bandwidth. Therefore, for a fixed received power, pushing symbol rates higher eventually reduces SNR unless optical power or collection efficiency is also improved. This bandwidth SNR trade off strongly informs the design choice to begin with modest data rates and a robust decode path before attempting high speed modulation.

3 Literature Review

3.1 UOWC in the Underwater Communications Landscape

Underwater communication technologies are typically divided into acoustic, radio frequency or magnetic induction, and optical approaches. Acoustic systems provide the longest ranges, often up to tens of kilometres, but they are constrained by low bandwidth, high latency due to the relatively slow speed of sound in water, and severe multipath effects. RF signals are strongly attenuated in conductive seawater, restricting practical range unless very low frequencies or specialised inductive couplers are used. Optical links occupy the short range, high throughput region. They can deliver high data rates with low latency and immunity to electromagnetic interference, but they require line of sight or favourable scattering conditions (Kaushal and Kaddoum, 2016).

UOWC links encode information on a light beam that propagates through water. Compared with acoustic and RF methods, UOWC offers higher data rates, lower latency, reduced power consumption, and immunity to electromagnetic interference. These benefits make UOWC attractive for real time applications such as remotely operated vehicle control, sensor data offload, diver communication, and short range underwater sensor networks. However, the underwater optical channel is highly susceptible to absorption, scattering, turbulence, and background light. The effective range depends heavily on water type: clear water may permit tens of metres of transmission, while turbid harbour water may restrict range to only a few metres.

The underwater channel experiences attenuation due to both absorption and scattering. Absorption converts photons into heat and increases rapidly outside the blue green region, whereas scattering deflects photons out of the receiver's field of view. Both mechanisms depend strongly on wavelength and particle size. The Beer Lambert law describes the exponential decay of optical intensity with distance and wavelength. Figure 3.1 illustrates the absorption and scattering coefficients across the visible spectrum. Attenuation is generally low between roughly 400–550 nm, which defines the useful blue green window for UOWC. To maximise received power, transmitters use high power blue green LEDs or lasers with collimating optics, and receivers employ lenses and narrow optical bandpass filters to reject background light.

Several modulation schemes have been investigated for UOWC. On Off Keying and Pulse Position Modulation are attractive for low cost LED systems because they are simple to implement and robust. Higher order schemes such as

phase shift keying, quadrature amplitude modulation, and OFDM can achieve much higher data rates under controlled laboratory conditions, but they require higher signal to noise ratio, more linear transmitters, and more complex receivers. For this project, a simple LED based IM/DD approach was selected because the focus was on producing a practical and repeatable underwater link rather than a maximum data rate demonstration.

3.2 Historical Background

Underwater communication using sound has been studied since the early twentieth century, particularly because of naval requirements during the World Wars. Acoustic communication became the dominant method for long range subsea links. Optical techniques for undersea communication emerged later, once lasers and solid state optoelectronics became available. Early experiments in the 1990s demonstrated the feasibility of underwater optical communication. For example, Snow et al. used a 514 nm argon ion laser to transmit data at 50 Mbit/s across a 9 m path in clear water. Significant progress occurred during the 2000s as improved lasers, detectors, and modulation schemes were developed. Later work reported multi-megabit and gigabit class links over controlled water paths. These early achievements set the stage for continued development of UOWC in both academic and industrial contexts.

3.3 Wavelength Selection and Water Types

Wavelength selection is central to UOWC because attenuation is wavelength dependent. Pure water absorption is relatively low in the blue green band, with a minimum in the visible region, while absorption increases toward red and infrared wavelengths (Pope and Fry, 1997). In real waters, dissolved organic matter, phytoplankton, sediment, and suspended particles introduce additional absorption and scattering.

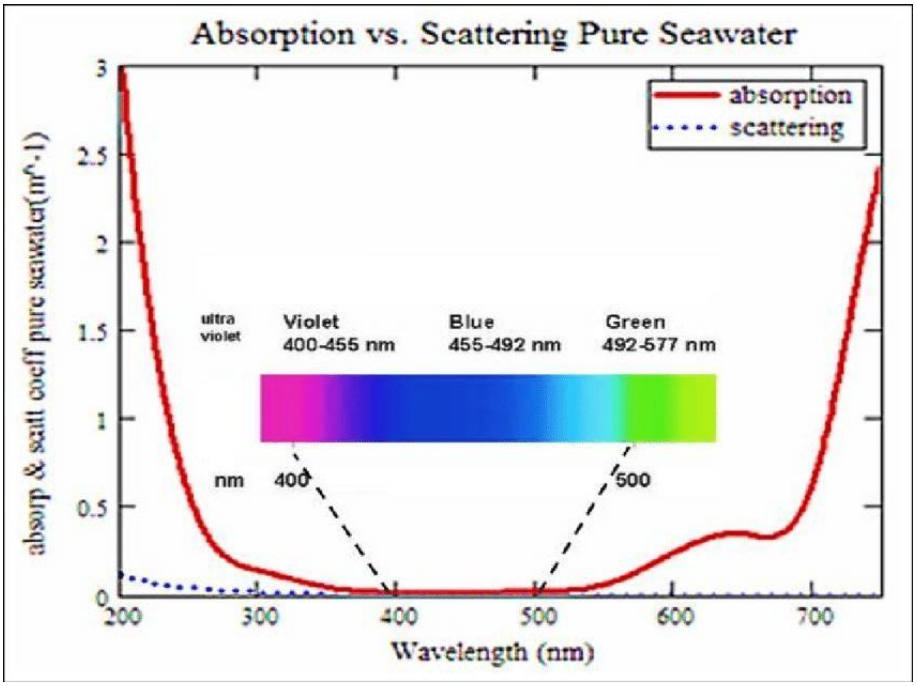

Figure 3.1: Absorption and scattering versus wavelength.

The design implication is that a wavelength that is optimal in clear ocean water may not remain optimal in coastal or turbid water. Testing should therefore span multiple effective attenuation conditions. In this project, blue and green LEDs in the approximate 448–530 nm range were selected to align with the low attenuation window described in the literature (Kaushal and Kaddoum, 2016). The final practical tests compared royal blue, blue, and green LEDs in harbour and coastal water samples to observe how real water conditions affected wavelength performance.

3.4 Transmitters: LEDs Versus Lasers

Transmitters for UOWC include LEDs and lasers. Lasers provide high optical power density, narrow spectral width, and good collimation, enabling longer ranges and higher data rates in controlled conditions. However, lasers introduce higher cost, stricter safety constraints, and more complex pointing and stability requirements. LEDs are lower cost, safer at comparable average power, mechanically robust, and easier to integrate, but they have wider spectral emission and broader divergence, which increases geometric loss unless optics are used.

Given the laboratory setting and project constraints, this system used high brightness blue and green LEDs with a constant current driver. This aligns with the practical prototype pathway highlighted in UOWC reviews, where LED

based systems are favoured for low cost short range links (Schirripa Spagnolo, Cozzella and Leccese, 2020).

3.5 Receivers: Photodiode Physics, Noise and Optical Filtering

3.5.1 Blue Green Responsivity Challenge

Standard silicon photodiodes typically exhibit peak responsivity in the near infrared, while blue green photons are absorbed very close to the silicon surface. In many generic devices, surface layers such as metalisation, heavy doping, and passivation form a region where carriers can recombine before they are collected. This reduces responsivity in the blue green band. Short wavelength or visible enhanced photodiodes are engineered to improve carrier collection near the surface and are therefore preferred for blue green UOWC.

3.5.2 APD Versus PIN Trade Off

Several Hamamatsu short wavelength silicon APDs were evaluated because APD gain can improve sensitivity at low received power. However, APDs require high bias voltages and careful noise management, and their cost and integration complexity are significant for a first prototype. For this reason, APDs were documented as evaluated but rejected for the baseline build. The selected baseline detector was a silicon PIN photodiode, the Hamamatsu S5973-02, which offers low bias complexity and lower cost while still supporting high speed operation when paired with an appropriate transimpedance front end. This decision does not exclude APD upgrades later; instead, the PIN receiver established a repeatable methodology before higher complexity receiver designs are considered.

3.5.3 Photodiode Selection

Selecting a photodiode for blue green UOWC is not straightforward. Most standard silicon photodiodes are designed to work best in the near infrared, with peak sensitivity around 800–950 nm. In the blue green band required for UOWC, silicon absorbs light within a very thin layer at the front surface. In many standard photodiodes this front region is not designed to collect charge efficiently, so carriers generated by blue green photons tend to recombine before being swept into the active region. From the outside this appears as poor responsivity in exactly the wavelength region where seawater is most transparent.

For that reason, the focus of this project was on short wavelength or violet enhanced devices, where the junction and coatings are optimised so that shallow generated carriers are collected rather than lost. For the receiver, two detector classes were considered: avalanche photodiodes and PIN photodiodes. APDs include internal gain, which is useful for very weak signals, but they require high voltage bias, careful temperature control, and higher cost. PIN photodiodes are simpler, lower cost, run at low bias voltages, and can still provide sufficient sensitivity for short range links when paired with a well designed transimpedance amplifier. Active area also creates a trade off: large area detectors are more forgiving of misalignment and collect more signal, but they also collect more background light and have higher capacitance. Small area detectors require better pointing but naturally reject ambient light and typically have lower capacitance, supporting higher bandwidth.

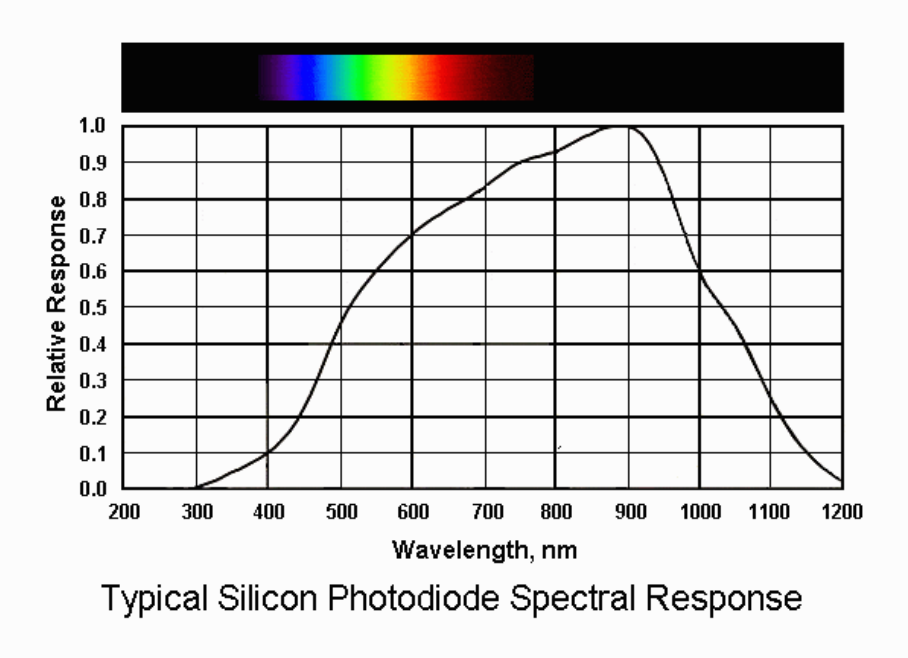

Figure 3.2: Typical silicon photodiode response versus wavelength.

3.5.4 Dark Current and Why It Matters

Dark current is the leakage current that flows through the photodiode even when no light is present, caused by thermally generated carriers in the depletion region. In the receiver, it behaves like a constant false light level plus associated shot noise. A high dark current raises the noise floor seen by the TIA, meaning the smallest detectable optical signal must be larger. In other words, lower dark current improves sensitivity and reduces bit error rate for a given received optical power. This is one of the reasons the design preference shifted away from large area APDs with higher leakage currents toward smaller area, lower

leakage parts (Hamamatsu Photonics, n.d.).

3.6 Modulation, Coding and Channel Modelling

The literature reports a wide range of modulation and coding approaches, from simple OOK and PPM to OFDM variants and advanced equalisation. For an IM/DD LED link, OOK and low order PPM offer a good starting point due to simplicity and ease of microcontroller implementation. More advanced schemes can be considered once the optical and analogue front end are stable. Channel modelling in many papers combines deterministic attenuation with stochastic fading to represent turbulence and scattering. In this project, modelling begins with Beer Lambert attenuation and then introduces effective loss terms for misalignment and scattering. This approach supports early design space exploration and provides a basis for later calibration using measurements (Weiskerger et al., 2018).

3.6.1 On/Off Keying

In OOK, a logic one is transmitted as light ON and a logic zero is transmitted as light OFF, so the electrical data stream becomes a rectangular optical waveform. OOK is hardware simple, tolerant of modest timing error, and widely used as a baseline in LED UOWC links. Its weakness is background sensitivity: because the receiver is effectively listening continuously, ambient illumination raises the DC level and increases shot noise, making zeros and ones harder to separate.

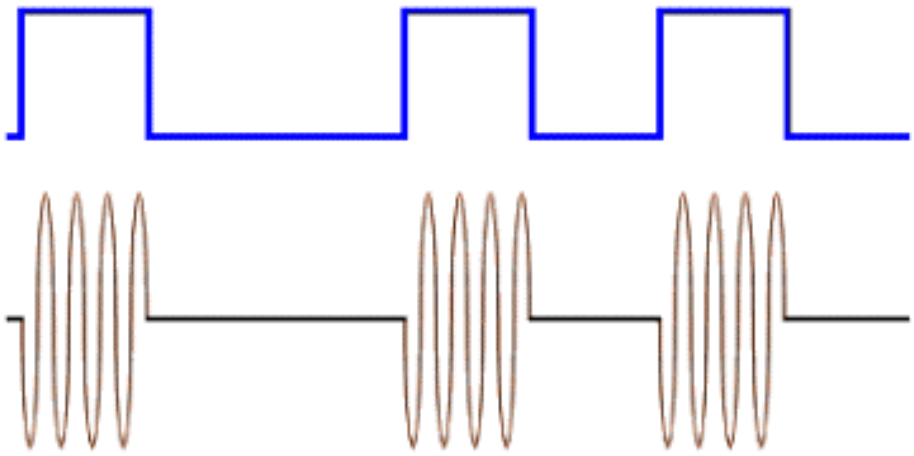

Figure 3.3: OOK and digital equivalent representation.

3.6.2 Pulse Position Modulation

PPM encodes information in the position of short, high power pulses within a wider frame. Only one narrow pulse is sent per symbol and the LED remains off for the rest of the frame. This improves power efficiency and can make the signal easier to distinguish from slow varying background light. The trade off is higher bandwidth and tighter synchronisation requirements, but in noisy or longer UOWC channels PPM can provide improved BER for the same average optical power.

3.6.3 Advanced Modulation

While simple schemes like OOK and low order PPM are common in practical UOWC links due to their robustness, advanced modulation formats such as M-QAM and OFDM can achieve much higher spectral efficiency under ideal conditions. In laboratory tank tests with clear water and stable alignment, researchers have demonstrated multi-gigabit per second optical links using high order QAM and OFDM. For example, a 16-QAM OFDM system at 450 nm achieved 4.8 Gbit/s over 5 m (Oubei et al., 2015). In M-QAM, each symbol carries multiple bits using distinct amplitude and phase combinations. OFDM sends data in parallel across many tightly spaced subcarriers, each of which can be modulated and equalised separately. However, these high rate formats require high SNR, precise channel knowledge, high linearity, and stable alignment. For this project, advanced modulation is treated as a future direction rather than part of the final prototype.

3.6.4 Beam Shaping and Spatial Diversity

Beyond modulation and coding, some recent UOWC work improves robustness by changing the spatial structure of the transmitted beam or by using multiple transmit and receive apertures. One example is the use of Airy beams, whose transverse field profile is described by the Airy function. In optics, engineered Airy beams can exhibit quasi non-diffracting behaviour over a finite distance, a self-bending trajectory, and self-healing after partial obstruction. For UOWC, these properties are attractive because underwater links often suffer from partial blockage, bubbles, particles, and turbulence induced beam wandering. The trade off is complexity, because generating an Airy beam requires additional beam shaping optics such as phase masks, spatial light modulators, or metasurfaces (Hu et al., 2024).

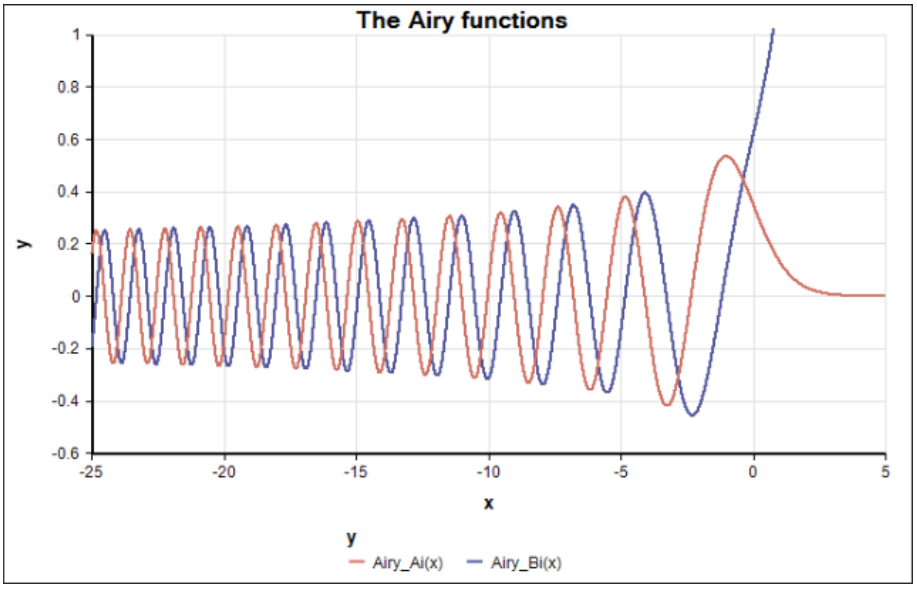

Figure 3.4: Airy function example.

A second spatial approach is MIMO, where multiple LEDs or lasers and multiple photodiodes or imaging receiver elements are used to improve reliability or increase throughput. In underwater channels, MIMO can reduce sensitivity to pointing and fading by providing redundant capture paths. However, it introduces practical challenges because the channels may not be fully independent due to scattering, and inter-channel interference can occur unless transmitter spacing, optics, and receiver segmentation are carefully designed. Overall, Airy beam shaping and MIMO represent next step techniques above the baseline LED IM/DD link used in this project (Chen et al., 2025).

3.7 Error Correction

To combat high error rates in turbulent or lossy channels, forward error correction can be used. Modern UOWC designs often pair advanced modulation with codes such as Reed Solomon or low density parity check codes. These codes add redundancy so that the receiver can detect and correct bit errors caused by fading and noise. In a future version of this project, a simple cyclic redundancy check or parity method could be added first, followed by more advanced block coding if required. An adaptive strategy may also be possible, where the system switches between simple OOK/PPM in poor conditions and higher rate schemes in clear and stable conditions.

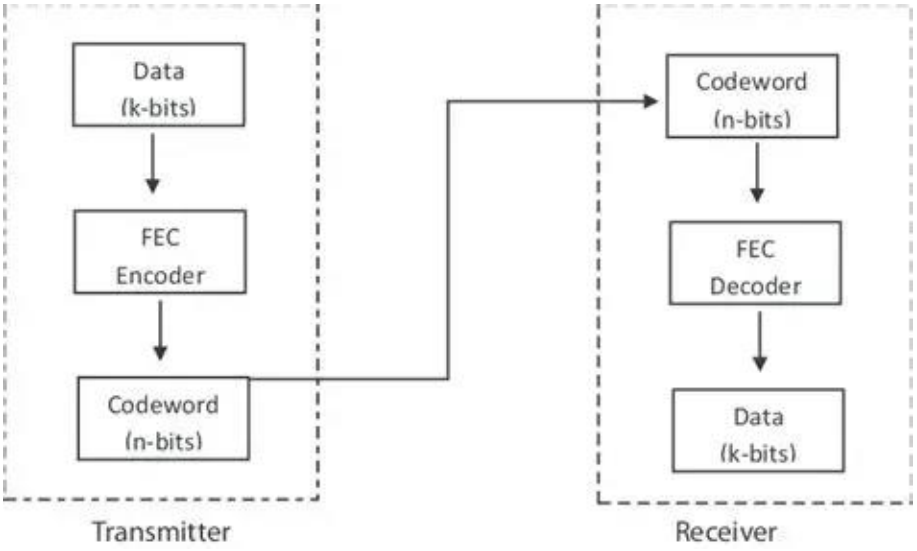

Figure 3.5: Forward error correction link concept.

3.8 Filtering Strategies

The receiver front end can use three complementary filtering strategies: spectral, spatial, and temporal filtering. In practice, spectral and spatial filtering prevent saturation and reduce background current; temporal gating then further suppresses remaining continuous background so OOK or PPM pulses stand out clearly. Overall, performance is set by how modulation and filtering are co-designed. Blue green LEDs and short wavelength detectors align the link with the low loss window of water; OOK provides a simple baseline; PPM offers a power efficient upgrade; and spectral, spatial, and temporal filtering protect the receiver from ambient light while exploiting the pulsed signal structure.

3.8.1 Spectral Filtering

Spectral filtering uses narrowband interference filters centred on each LED channel, such as 450 nm, 470 nm, and 530 nm with an approximate ±10 nm bandwidth. This allows light in the desired blue green band to reach the detector while rejecting much of the out of band ambient illumination from lamps or sunlight.

3.8.2 Spatial Filtering

Spatial filtering is implemented through lens choice, mechanical layout, baffles, apertures, and receiver field of view control. A lens can collect light from a limited field of view and focus it onto the photodiode, while baffles and apertures restrict off-axis light. This increases the collected signal from the transmitter

direction while rejecting much of the isotropic background and tank reflections.

3.8.3 Temporal Filtering

Temporal filtering exploits the pulsed nature of OOK and especially PPM. In a time gated receiver, the detector or software decision process is only open during the window when a symbol or pulse is expected. For OOK this can be as simple as sampling near the middle of each bit period; for PPM the gate aligns with the candidate time slot. This reduces background induced noise and improves BER in noisy conditions.

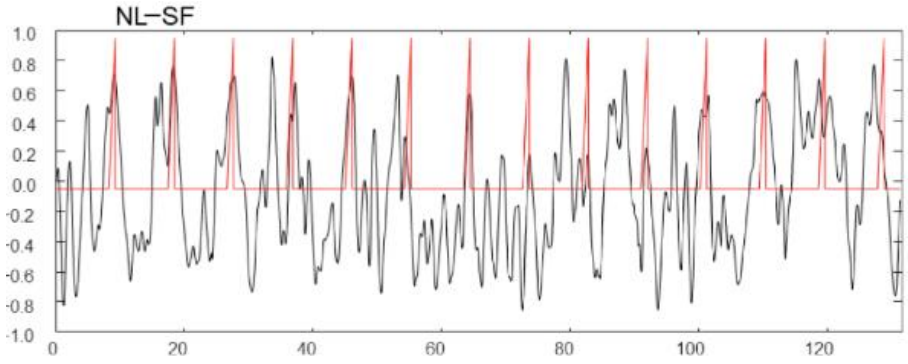

Figure 3.6: Temporal filtering and noise concept.

3.9 Summary and Research Gap

The literature shows that UOWC fills a clear niche between acoustic and RF approaches: it offers high throughput and low latency over short ranges, but performance is strongly limited by the underwater channel and practical system constraints. Link range is set primarily by wavelength dependent absorption and scattering, while real world robustness is dominated by ambient light, misalignment sensitivity, receiver noise, bandwidth trade offs, and mechanical stability. Many studies demonstrate impressive rates using lasers and high order modulation in controlled conditions, but LED based links remain a realistic pathway for low cost laboratory and fieldable prototypes.

A consistent theme across UOWC work is that successful prototypes are co-designed systems. Wavelength selection, transmitter optics, receiver aperture, detector choice, analogue front end design, filtering, and decoding must be chosen together because each trade off affects both signal and noise. The gap addressed by this project is not another isolated maximum data rate demonstration, but a repeatable engineering methodology that connects a tractable channel model, justified hardware choices, and a robust decode path under realistic laboratory and field conditions. The contribution is a baseline platform

that prioritises reliability first: a blue green LED transmitter with controlled drive, a cost appropriate PIN photodiode receiver, comparator threshold detection, and a practical testing method for real water samples.

4 Requirements and Specification

This chapter translates the project aim into specific requirements that were used to guide the design, implementation, and testing of the prototype. The requirements are divided into functional, performance, and practical constraints. Each requirement was verified through bench testing, underwater testing, oscilloscope measurements, serial logging, or design review.

4.1 Functional Requirements

Requirement	Verification method
Transmit digital data using visible light intensity modulation.	Firmware test, oscilloscope verification, and serial output.
Receive and detect optical data using a photodiode based receiver.	Oscilloscope measurement and comparator output verification.
Convert weak analogue optical pulses into usable digital logic signals.	IDAC threshold testing and comparator output comparison.
Operate in the 450–550 nm blue green window.	LED selection and wavelength comparison tests.
Demonstrate underwater optical communication through a water filled test rig.	Tap water, harbour water, and coastal water trials.
Compare wavelength performance in different water samples.	IDAC threshold margin measurements for green, blue, and royal blue LEDs.
Identify the practical data rate limitations of the system.	Baud rate testing at multiple UART speeds.
Reduce ambient light sensitivity through enclosure design and threshold control.	Shielded pipe testing and comparator threshold adjustment.
Keep the system low cost and suitable for student project development.	Component selection and design review.

Table 4.1: Functional requirements and verification methods.

4.2 Design Constraints and Assumptions

The final prototype was constrained by available components, cost, laboratory safety, mechanical robustness, and the time available for construction and testing. The transmitter output was limited by the TPS92612 LED driver, the available supply voltage, LED thermal limits, and the need to keep the optical output safe for practical handling. The receiver was constrained by the photodiode sensitivity, amplifier bandwidth, comparator threshold stability, and the analogue resources available on the PSoC platform.

The optical channel was modelled using Beer Lambert attenuation as a first order approximation. This allowed the main effect of water absorption and scattering to be represented, but it did not fully account for bubbles, turbulence, internal pipe reflections, changing ambient light, or complex scattering behaviour. These additional effects were instead investigated practically during underwater testing.

The PVC pipe test rig improved alignment and reduced ambient light, but it also introduced reflections that affected communication at higher baud rates. Therefore, the test rig was treated as both a controlled optical path and a practical limitation of the experiment.

5 System Design and Methodology

5.1 System Overview

The UOWC system consists of a digital transmitter, an optical transmitter, an underwater optical channel, and a receiver chain. The transmitter uses a PSoC microcontroller to generate UART based digital data, which drives a TPS92612 constant current LED driver. The optical output is produced by interchangeable royal blue, blue, and green LEDs. The transmitted light then propagates through the water filled test path.

At the receiver, a silicon photodiode and transimpedance amplifier convert the received optical signal into a voltage. This analogue signal is then applied to a comparator, where it is compared against an adjustable threshold generated using the PSoC IDAC. When the received optical pulse exceeds the selected baseline, the comparator produces a full swing digital output suitable for microcontroller detection. This architecture separates weak analogue signal detection from digital decoding and was essential to improving the practical range of the system.

Figure 5.1 shows the high level system architecture used for both the prototype and simulation model.

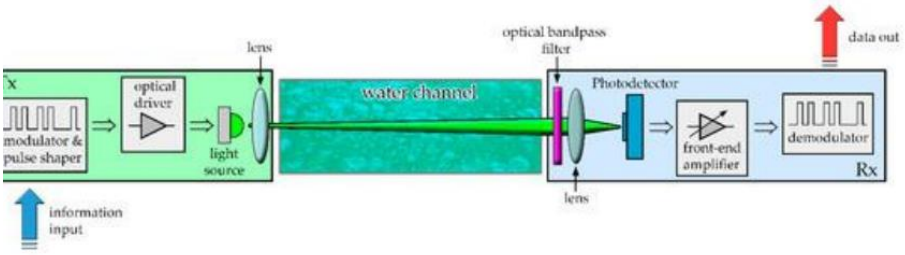

Figure 5.1: Proposed system diagram.

5.2 System Development Methodology

The methodology for this project followed an iterative design, build, test, and refine approach. Rather than developing the underwater link as a single complete system from the beginning, each major subsystem was first tested independently and then gradually integrated into the final prototype. This made it easier to isolate faults and determine whether issues were caused by the transmitter, receiver, firmware, power supply, optical alignment, or mechanical enclosure.

The first stage involved defining the system architecture from the theory and literature review. This established the use of a blue green LED transmitter,

intensity modulation, direct photodiode detection, analogue signal conditioning, and embedded threshold detection. Component choices were then made around practical constraints such as cost, availability, safe optical power, driver compatibility, receiver sensitivity, and ease of integration.

The second stage focused on bench testing. The LED driver, photodiode receiver, UART communication, and comparator thresholding were tested in air before underwater trials were attempted. Oscilloscope measurements and serial output were used throughout this stage to compare the transmitted signal, the raw receiver waveform, and the recovered digital output. This testing showed that direct UART reception was too dependent on the analogue signal reaching a valid logic level, leading to the use of the comparator and IDAC threshold method.

The third stage involved mechanical and environmental integration. The transmitter and receiver were mounted in a PVC pipe test rig to create a fixed optical path through water. Waterproofing, cable sealing, alignment, and support structures were added as the project moved from bench testing to real water testing. This stage showed that mechanical design had a direct effect on communication reliability.

The final stage was experimental evaluation. The completed prototype was tested in different water samples and with different LED wavelengths. The IDAC comparator threshold was used as a practical signal margin indicator, allowing the relative performance of royal blue, blue, and green LEDs to be compared under the same receiver conditions. The results from these tests were then used to evaluate the system limitations and identify future improvements.

5.3 Transmitter Design

The transmitter is built around a high brightness blue or green LED driven by a constant current LED driver, the Texas Instruments TPS92612-Q1. Constant current drive provides predictable optical output and reduces nonlinearities associated with the LED current-voltage characteristic. The driver is controlled by the PSoC microcontroller, which generates the modulation waveform and packet data.

LED selection was guided by the water transmission window and by practical packaging, thermal, and driver current limits. During early integration, a mismatch was identified in the original LED selection, and the design was updated to target the LUXEON 3535L colour line family. The TPS92612-Q1 supports up to 150 mA output current, which is consistent with laboratory operation and thermal safety management. The selected LEDs allowed the project to

compare wavelengths while staying within the driver capability.

5.3.1 LED Selection and Driver Integration

The project originally considered Lumileds LUXEON Rebel Color high power LEDs, specifically Royal Blue, Blue, and Green devices. These LEDs are rated for relatively high drive currents and have forward voltage drops around 3.0–3.4 V at typical operating currents. However, mathematical testing with the Texas Instruments TPS92612-Q1 LED driver showed that these LEDs were not well matched to the selected driver. The TPS92612-Q1 is a linear high side driver limited to approximately 150 mA output current and regulates current through a 98 mV drop across a sense resistor. Under these constraints, the Rebel LEDs would be under-driven and the driver would operate close to its headroom limits.

To resolve this, the design migrated to the LUXEON 3535L Color Line LEDs, which better match the driver's operating range. Three mid power SMD emitters were selected: royal blue at approximately 448 nm using L135-U450003500000, blue at approximately 475 nm using L135-B475003500000, and green at approximately 530 nm using L135-G525003500000. These devices have typical forward voltages that are suitable for 100–150 mA operation and are therefore compatible with the TPS92612-Q1 driver.

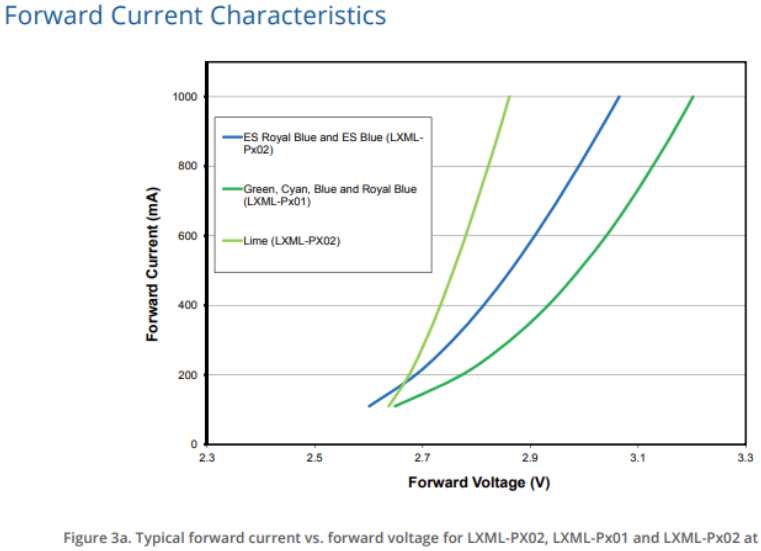

Figure 5.2: Forward current comparison for the original LED option.

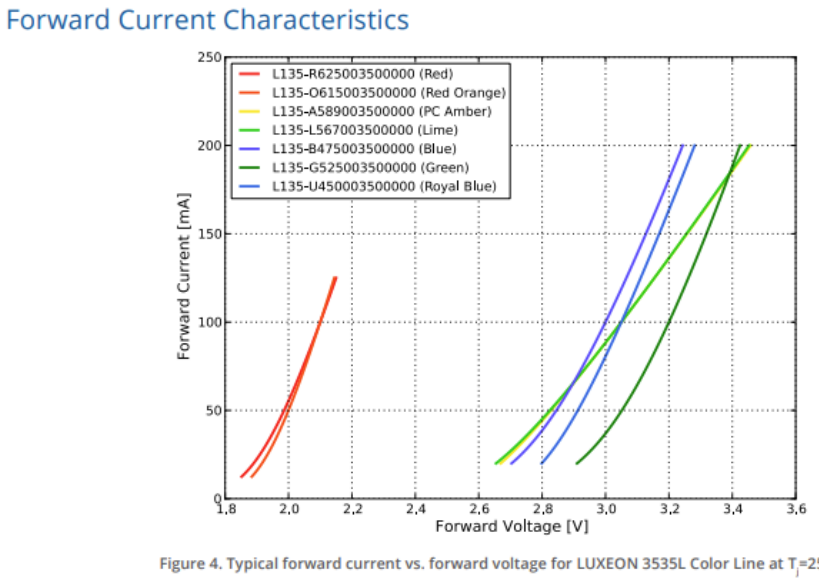

Figure 5.3: Forward current comparison for the selected LUXEON 3535L LEDs.

The switch to the LUXEON 3535L LEDs provided several benefits. The LEDs operate efficiently within the TPS92612 current range, their forward voltage remains suitable for the available supply voltage, and they provide sufficient optical output for short range testing. Their wide Lambertian radiation pattern also relaxed alignment requirements, which was useful during practical field testing.

5.4 Receiver Design

The receiver was designed to convert small changes in received optical power into a reliable digital signal. The final receiver chain consisted of a photodiode, a transimpedance amplifier, a comparator, an adjustable IDAC threshold, and PSoC based digital processing.

The selected baseline detector was the Hamamatsu S5973-02 silicon PIN photodiode. This device was chosen because it has good short wavelength response, low bias complexity, relatively low dark current, and a small active area that helps reduce ambient light collection. Hamamatsu short wavelength APDs were also evaluated because their internal gain could improve sensitivity, but they were not selected for the final prototype due to their higher cost, high voltage bias requirements, additional noise considerations, and greater integration complexity.

The photodiode current was converted into a voltage using a transimpedance amplifier. Early direct UART tests showed that the analogue output often contained visible optical pulses, but these pulses were not always large enough to meet the digital logic threshold of the UART input. To solve this,

the receiver was changed to a comparator based decision stage. The photodiode/TIA output was connected to the positive comparator input, while the PSoC IDAC generated an adjustable reference voltage on the negative input. This allowed weak optical pulses to be converted into full swing digital transitions whenever they exceeded the selected threshold.

The receiver design was therefore based on three key principles: maximise useful received signal, reject ambient light where possible, and use a programmable threshold to recover digital transitions from weak analogue pulses.

5.5 Photodetector Evaluation and Selection

Table 5.1 summarises the evaluation logic for candidate detectors. APDs provide internal gain but require careful biasing and can introduce excess noise and complexity. PIN photodiodes provide linear response with low bias voltage, enabling rapid prototyping and lower cost.

Device class	Example parts	Pros	Cons	Decision
Si APD, short wavelength	Hamamatsu S12053 series; S5345	High sensitivity through internal gain; visible enhanced versions available.	High bias voltage; higher cost; more integration risk; excess noise.	Evaluated but rejected for baseline; possible future upgrade.
Si PIN photodiode	Hamamatsu S5973-02	Low bias; low cost; high speed; simpler analogue front end.	Lower sensitivity than APD; relies on optics and TIA gain.	Selected baseline device.

Table 5.1: Summary of photodetector options.

The Hamamatsu S5345 large area short wavelength APD was first considered. Its 5 mm active area would make alignment in a tank easier and its internal avalanche gain would help with weak signals. However, the large junction area introduces higher capacitance and dark current, limiting bandwidth and increasing noise. It also requires a high bias voltage and is relatively expensive for a

student project. The Hamamatsu S12053-05, a smaller 0.5 mm short wavelength APD, was also considered. It offers better capacitance and dark current performance while retaining avalanche gain, but still requires a high voltage bias supply and specialist integration.

The final choice for this prototype was the Hamamatsu S5973-02 violet enhanced silicon PIN photodiode. Although it does not provide internal gain, it has strong blue response and is suitable for high speed operation when paired with a low noise TIA. Its small active area helps reduce capacitance and limits the amount of ambient light reaching the detector. Combined with low voltage operation and lower cost, the S5973-02 offered the best price-performance trade off for this stage of the project.

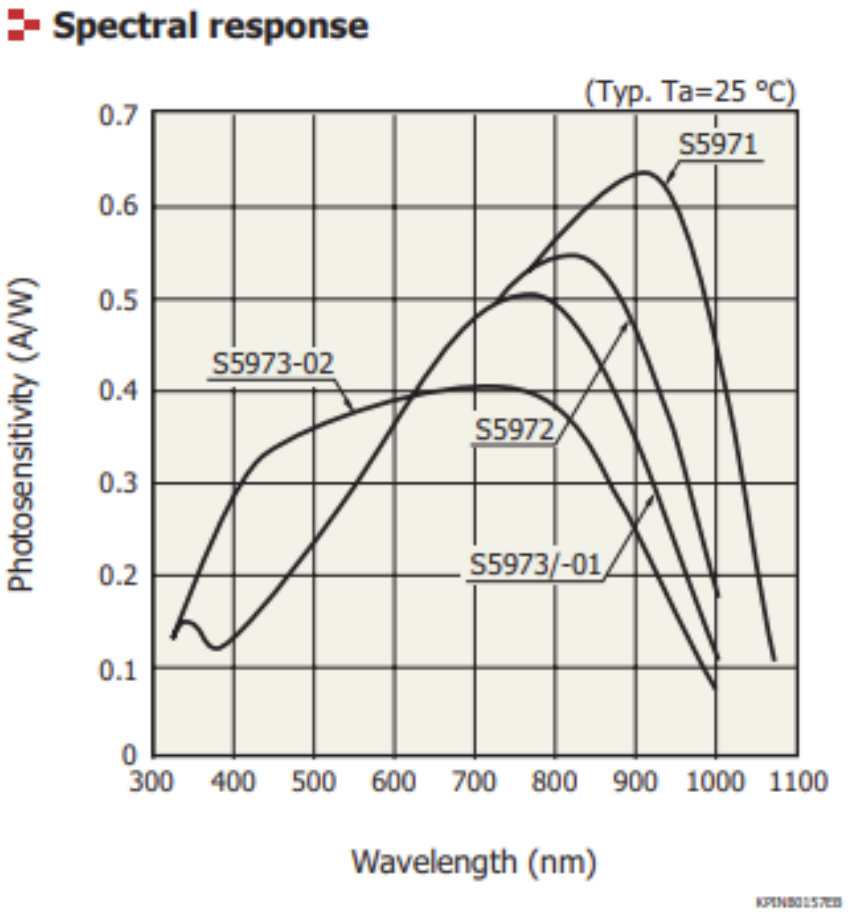

Figure 5.4: Hamamatsu photodiode spectral responsivity.

5.6 Modulation

Modulation and filtering are tightly linked in the design of an LED based UOWC receiver. This project used intensity modulation and direct detection, primarily in an OOK style format, because it maps naturally onto driving a blue green

LED and detecting it with a silicon photodiode. More advanced schemes such as PPM are identified as future improvements once the basic link has been made more repeatable.

5.7 Firmware Architecture and Synchronisation

The firmware is organised around a simple deterministic transmitter and a receiver that prioritises reliable synchronisation. On the transmit side, the PSoC generates UART based serial data that drives the LED driver. A packet structure with a recognisable header, numeric payload, and tail was developed during testing so that received messages could be checked for basic validity.

On the receive side, the key requirement was to convert the analogue photodiode signal into a clean digital waveform before decoding. The photodiode and TIA produce a voltage proportional to received light, but that signal includes ambient light offsets, noise, and slow drift. Using the ADC and a single threshold in firmware was useful for debugging but was sensitive to timing drift and noise. The improved approach was to condition the TIA output with a comparator so that it becomes a stable logic level signal with clean transitions.

The PSoC hardware UART remains useful because it is designed to detect the start bit edge and then sample subsequent bits near the centre of their bit periods. This avoids the main timing problem seen during early software thresholding, where one transmitted high pulse could be counted multiple times if sampled at the wrong phase. In the final system, the comparator and IDAC method therefore formed the bridge between the analogue optical receiver and the digital UART based communication logic.

5.8 Bill of Materials

Component	Supplier	Stock number	Price	Qty
Royal Blue LED, 450 nm	Digi-Key	L135-U450003500000	$0.97	1
Blue LED, 475 nm	Digi-Key	L135-B475003500000	$1.01	1
Green LED, 530 nm	Digi-Key	L135-G525003500000	$1.01	1
SMD 1206 resistor, 1 ■	Farnell	ERJ8GEYJ1R0V	$0.40	1
2.7 ■ Metal Film Resistor	Rs Online	150-666	$1.55	1
Photodiode	Rs Online	124-7158	€7.91	1
PVC Pipe	Woodies	N/A	$30	1
Extension cable	Halfords	N/A	$10	1
PVC Top	Halfords	N/A	$5	1
PVC Connector	Halfords	N/A	$5	1
Electrical gromit	Halfords	N/A	$5	1
PSoC 4	Rs Online	124-4183	$32.07	2

Table 5.2: Bill of materials.

5.9 UOWC KiCad Schematic

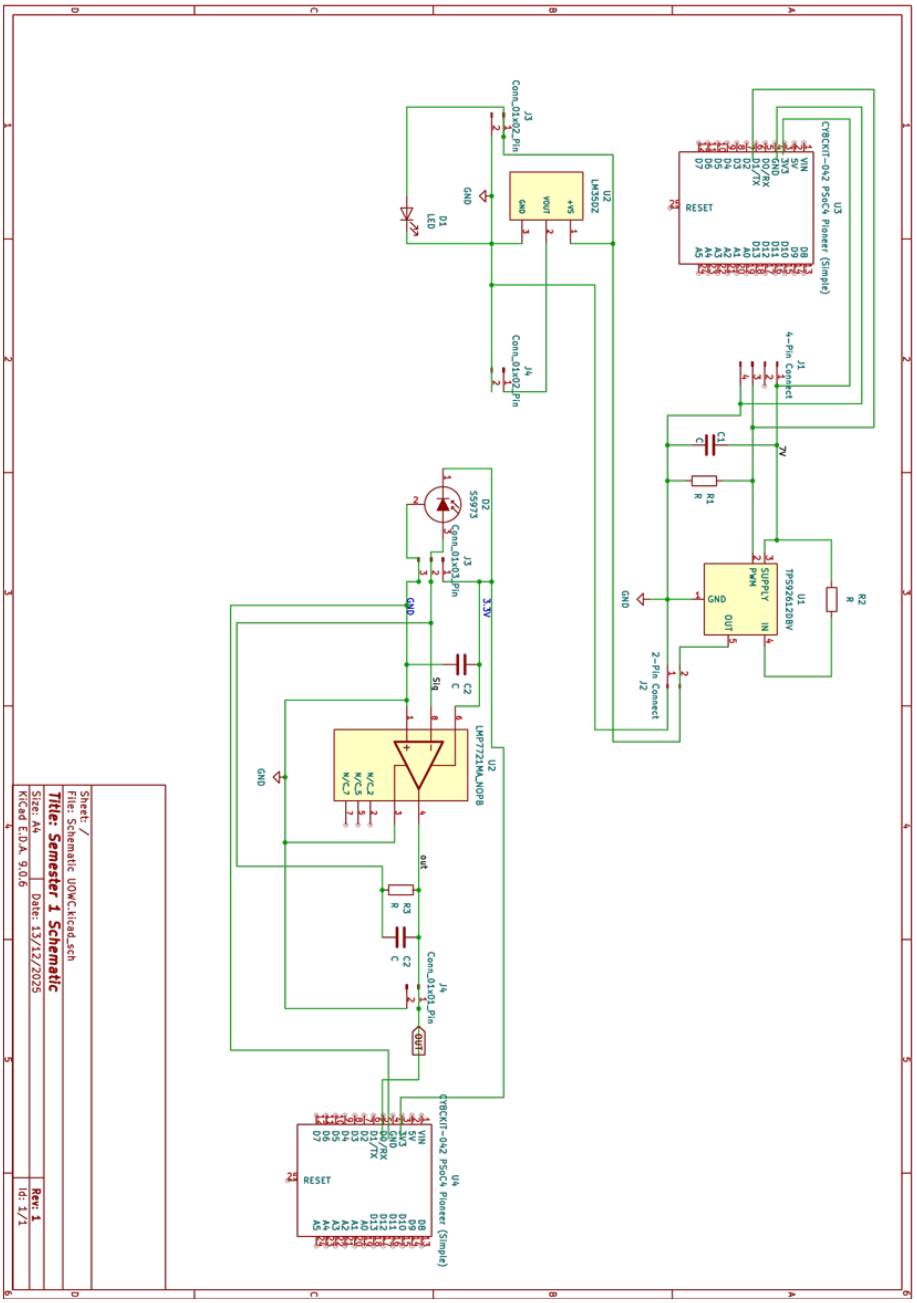

Figure 5.5: KiCad schematic.

6 Simulation and Modelling

The underwater optical communication simulation model was developed in Python and stored in a GitHub repository as part of the technical development of this project. The model was created as an engineering tool to estimate how the optical link behaves as distance, water type, wavelength, receiver sensitivity, baud rate, and pipe geometry are changed. Rather than acting as a final fully calibrated prediction tool, the simulation provides a useful way to compare design choices and understand which parameters have the greatest effect on the received signal.

The current version of the repository includes a command line interface that can run simulations using built in LED presets, receiver presets, water presets, baud rate settings, and an optional glossy pipe total internal reflection model. This made the simulation more closely related to the practical test rig, as the experimental system used Lumileds blue, royal blue, and green LEDs, a Hamamatsu S5973-02 photodiode receiver, a PSoC based comparator stage, and a water filled pipe test section.

6.1 Beer Lambert Attenuation Model

The core channel model is based on the Beer Lambert attenuation law. This describes how optical power decreases exponentially as it travels through water. For a given path length d and wavelength λ, the received optical power is represented as:

$$P(d) = P_0 e^{-c(\lambda)d} \tag{6.1}$$

where P_0 is the transmitted optical power and $c(\lambda)$ is the beam attenuation coefficient. The attenuation coefficient is made up of absorption and scattering components:

$$c(\lambda) = \alpha(\lambda) + \beta(\lambda) \tag{6.2}$$

where $\alpha(\lambda)$ represents absorption and $\beta(\lambda)$ represents scattering. The simulation includes water presets such as pure sea, clear ocean, coastal ocean, and turbid harbour. These presets allow different water conditions to be compared without manually changing the absorption and scattering values each time.

In the practical project, this was important because underwater optical com-

munication is highly dependent on water quality. Clear coastal water can allow blue and royal blue wavelengths to travel further, while turbid harbour water causes stronger attenuation due to increased scattering and absorption. The model therefore gives a useful first estimate of how the link range changes between different water types.

6.2 Simulation Repository and Command Line Interface

The simulation repository is organised around a command line interface, allowing repeatable tests to be run from the terminal. The most relevant example run for this project is shown below:

```
python -m UOWC_SIM.uowc_sim.cli run --led blue --preset coastal_ocean
--pipe-tir --pipe-radius-m 0.012 --pipe-wall-reflectivity 0.985
--pipe-water-n 1.343 --pipe-wall-n 1.490 --pipe-coupling-efficiency 0.82
--pipe-max-gain 35 --baud 1200 --dmin 0.2 --dmax 5 --step 0.2
```

This command is significant because it represents the most realistic simulation case for the physical test rig. The blue LED option selects the Lumileds L135-B475003500000 configuration, representing a nominal wavelength of approximately 475 nm. The coastal ocean preset represents clearer seawater conditions, which are more relevant to the Ballybunion coastal tests than the turbid harbour case. The baud rate is set to 1200 baud because this was closer to the reliable data rate found during physical pipe testing, where higher baud rates were more affected by reflections and intersymbol interference.

The command also enables the pipe total internal reflection model. This is important because the laboratory test setup used a narrow water filled pipe, and the inside of the pipe did not behave like a completely open water channel. Reflections from the pipe wall and confinement of the light path affected the received signal. The simulation therefore includes pipe radius, wall reflectivity, refractive index, coupling efficiency, and a maximum guiding gain so that the model can represent this guided pipe behaviour more realistically than a simple free space spreading model.

6.3 System Definition

The model begins by defining the transmitter, receiver, water channel, turbulence model, noise model, distance grid, and optional pipe guiding parameters. For the LED based case, the transmitter includes optical power, wavelength, LED divergence, and transmitter efficiency. The receiver includes photodiode

area, responsivity, field of view, receiver efficiency, dark current, load resistance, bandwidth, and TIA gain.

The current receiver preset for the Hamamatsu S5973-02 includes the photodiode active area, responsivity, dark current, comparator output rails, TIA gain, and PSoC logic high threshold. This is useful because it connects the simulation to the actual receiver architecture used in the prototype. Instead of only estimating received optical power, the model also estimates the signal voltage that would be available at the simulated PSoC input.

6.4 Pipe Total Internal Reflection Model

A major improvement in the current version of the model is the inclusion of a glossy pipe guiding function. In the physical test rig, the transmitter and receiver were positioned along a pipe filled with water. This meant that some of the optical signal could be guided along the pipe by reflections, rather than spreading freely as it would in open water.

The pipe model estimates a guiding gain using the pipe radius, the beam angle, wall reflectivity, refractive indices, coupling efficiency, and an upper gain limit. The pipe radius in the example command is set to 0.12 m, giving an inner radius of 12 cm. The wall reflectivity is set to 0.985, representing a highly reflective inner boundary. The refractive index of water is set to 1.343 and the wall refractive index is set to 1.490. The coupling efficiency is set to 0.82, which accounts for imperfect launch of light into the pipe, and the maximum gain is limited to 35 so that the guiding effect remains physically constrained.

This model is still an approximation, but it is valuable because it acknowledges that the laboratory pipe setup is not identical to an open underwater channel. The pipe can increase the apparent received power by reducing geometric spreading, while at the same time introducing reflections that can distort the received pulses. This matches the experimental observation that 1200 baud worked more reliably than higher baud rates in the pipe, because delayed reflections had less effect at the lower data rate.

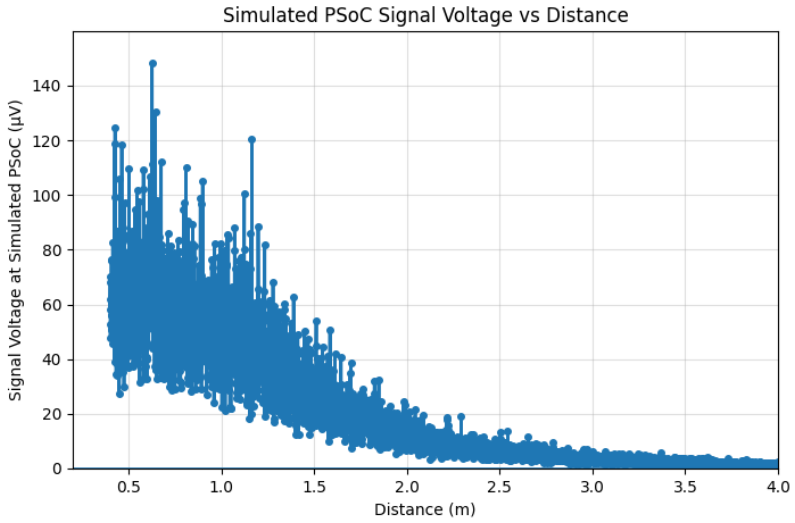

Figure 6.1: Simulated Signal attenuation vs distance (Varied at the start due to multipathing in test rig)

6.5 Signal Generation and Channel Impairments

The simulation represents the optical link using an on off keying style intensity modulation model. The received optical power is calculated by combining transmitter power, optical efficiency, Beer Lambert attenuation, geometric spreading, receiver collection area, field of view, turbulence effects, and the optional pipe guiding factor.

For an LED source, the model includes Lambertian emission behaviour and beam divergence. This is suitable for the practical transmitter because the project used LEDs rather than a tightly collimated laser diode. The blue LED case is particularly relevant because the experimental results showed that blue and royal blue wavelengths performed better than green in the coastal water tests.

6.6 Noise, SNR, BER, and Receiver Voltage

After calculating received optical power, the model converts this value into photocurrent using the photodiode responsivity. The simulated current is then converted into a receiver voltage using the load resistance and TIA gain. This is useful because the practical receiver does not only depend on received power; it depends on whether the signal at the receiver front end is large enough to cross the comparator threshold.

The noise model includes shot noise, thermal noise, dark current noise, and relative intensity noise. These are combined into a total noise variance, which

is then used to estimate signal to noise ratio and bit error rate. Although the BER value is approximate, it provides a useful comparison between different distances and water conditions. In this project, the BER curve is most useful as a trend indicator rather than an exact prediction of the measured serial link error rate.

The model also calculates simulated PSoC signal voltage, comparator output voltage, and digital logic interpretation. The comparator output is represented using low and high voltage rails, with a PSoC logic high threshold. This is important because the practical receiver used a comparator to convert the analogue photodiode signal into a digital signal suitable for UART style decoding.

6.7 Output and Visualisation

The simulation produces several plots and output files. These include received power versus distance, SNR versus distance, BER versus distance, simulated PSoC signal voltage versus distance, signal voltage with detection threshold, and comparator output with PSoC logic threshold. These plots allow the simulated optical and electrical behaviour to be inspected together.

The distance range in the example command is set from 0.2 m to 5 m in 0.2 m steps. This is suitable for the scale of the experimental test rig and the expected short range behaviour of the LED based underwater optical link. By keeping the distance range focused on the physical test scale, the plots are more useful for analysing the prototype rather than showing unrealistic long range behaviour.

Figure 6.2: Python command line example used to run the underwater optical link simulation.

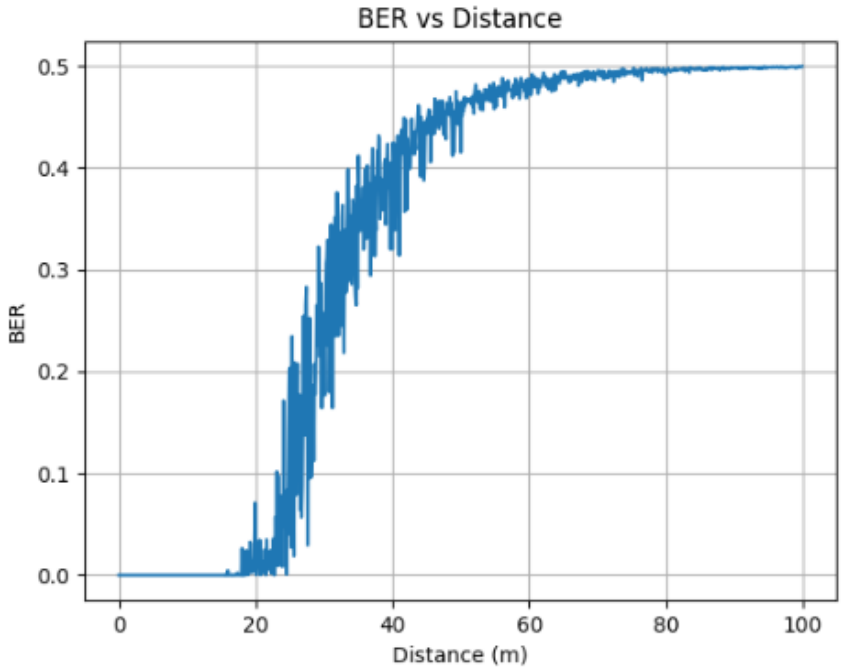

Figure 6.3: Simulated bit error rate versus distance.

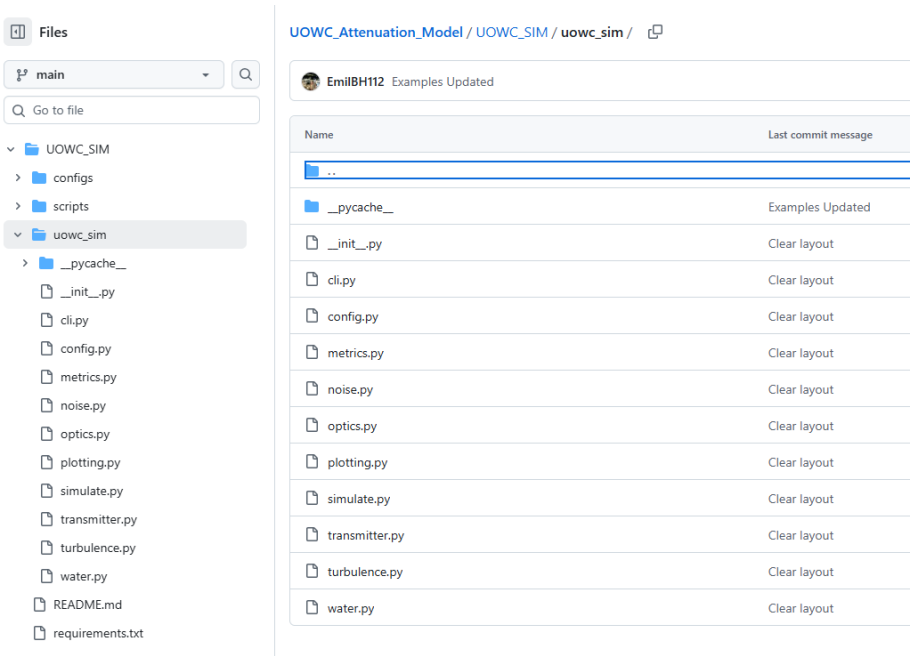

Figure 6.4: GitHub repository containing the Python simulation model.

UOWC_SIM — End-to-End Underwater Optical Wireless Communication Simulation

This repository implements an end-to-end UOWC simulation pipeline aligned with the two flowcharts provided and the formulas in the research paper:

- Zayed & Shokair (2025), "Modeling and simulation of optical wireless communication channels in IoUT considering water types, turbulence and transmitter selection" (Scientific Reports).

Features

- Modular pipeline following the flowcharts:
  i. Define system parameters (wavelength, water type, channel model, transmitter, receiver)
  ii. Generate optical signal (OOK default)
  iii. Apply channel impairments (absorption, scattering via Beer–Lambert, turbulence: log-normal / generalized-gamma / Weibull, noise: shot + thermal + dark + RIN)
  iv. Transmit through channel (geometry and optics; LED-PS vs LD-PS link budget)
  v. Compute metrics (Received power, SNR, BER, Data rate)
  vi. Analyze and visualize results (matplotlib)
  vii. Simple protocol optimization hints (choose source, power, FOV)
- Presets for water types (pure sea, clear ocean, coastal ocean, turbid harbor) at lambda=520 nm per Table 3 in the paper.
- Configuration first: edit `configs/*.yml` or pass CLI flags.
- CLI interface to pick scenario and run plots.
- Minimal dependencies: numpy, pyyaml, matplotlib.
- Optional glossy-pipe guiding model with total internal reflection (TIR) approximation to emulate waveguide-like confinement and longer effective signal reach.

> Note: Formulas implemented as in-paper equations: (7)-(10) noise, (16)/(22) received power for LED-PS / LD-PS, (18) Lambertian order, (19) receiver concentrator gain, (20)/(21) TX optics gain, (23) SNR, (24) BER ~= Q(sqrt(SNR)).

Figure 6.5: GitHub repository README.md

6.8 Model Validation and Calibration

The simulation was developed as an early engineering model rather than a fully calibrated representation of the final prototype. It was useful for exploring the effects of water type, wavelength, distance, receiver sensitivity, baud rate, and pipe reflections. However, the physical tests showed that several practical effects are difficult to model accurately without experimental calibration.

These effects include imperfect optical alignment, enclosure window losses, changing ambient light, internal pipe reflections, water clarity variations, comparator threshold adjustment, LED drive current variation, and the real frequency response of the receiver amplifier. The practical tests also showed that baud rate had a strong effect on reliability because delayed reflections inside

the pipe caused intersymbol interference at higher data rates.

Future calibration should use measured oscilloscope values from the receiver at known distances. These measurements could be used to fit an effective attenuation coefficient, coupling efficiency, and threshold margin. The most useful calibration approach would be to record received voltage versus distance for each LED wavelength, then adjust the model so that the simulated PSoC voltage follows the same trend as the measured data.

6.9 Current Limitations of the Repository

The current repository is useful, but it remains in an early development stage. A limitation is that the model still uses simplified optical power assumptions. The blue LED configuration uses an approximate electrical operating point, but future work should replace this with measured radiant optical power or a datasheet based radiant flux value at the actual drive current. This would make the received power and voltage predictions more accurate.

Despite limitations, the repository provides a strong foundation for modelling the underwater optical link. It connects the theoretical Beer Lambert attenuation model to practical hardware parameters such as LED wavelength, receiver responsivity, TIA gain, comparator threshold, baud rate, and pipe geometry. This makes it a useful design and analysis tool for the project, especially when comparing experimental results against expected trends.

6.10 Future Improvements

The model could be improved by adding measured photodiode amplifier gain, measured comparator thresholds, optical window losses, and more wavelength specific water attenuation values. The pipe model could also be improved by using measured reflection behaviour instead of an approximate guiding gain. A future version could also include pulse spreading and intersymbol interference so that baud rate reliability can be predicted more directly.

Overall, the simulation supports the experimental work by showing how received power, voltage, SNR, BER, and digital threshold behaviour are expected to change with distance. It does not replace physical testing, but it provides a useful link between theory and experiment

7 Implementation and Debugging

7.1 Hardware Progress

The implementation stage focused on developing a working transmitter drive chain, receiver front end, serial communication path, and testable optical link. On the transmitter side, a dedicated LED driver circuit was developed around the Texas Instruments TPS92612 to provide constant current drive for the selected LUXEON 3535L LEDs. The LED current was set using the driver's sense resistor relationship, allowing the optical output to be controlled more reliably than if the LED had been driven directly from a microcontroller pin.

On the receiver side, the system progressed from a simple photodiode and analogue readout arrangement to a comparator based threshold detector. Early testing showed that the photodiode and amplifier could detect optical pulses that were too small for direct UART decoding. This led to the use of the PSoC comparator and IDAC, which became one of the most important improvements in the project.

The project therefore moved from isolated transmitter and receiver tests to an end to end optical communication system. The firmware generated the transmitted data, the LED driver converted the signal into optical pulses, the photodiode receiver detected the light, and the comparator restored the received signal into a digital waveform suitable for further processing.

7.2 Receiver Sampling and Clock Alignment Issue

During early testing at low symbol rates, the receiver sometimes interpreted a single transmitted high as multiple high events. This behaviour was initially considered in terms of the Nyquist sampling criterion; however, the underlying cause was clock misalignment and sampling phase, not simply insufficient sampling rate. If the transmitter generates a pulse that remains high for a duration comparable to multiple receiver sample intervals, then depending on when sampling begins relative to the pulse, the receiver may record multiple consecutive samples above threshold. A naive decoder that treats each above threshold sample as a new symbol will therefore overcount.

The correct solution is to impose a symbol clock, recover timing from the transmitted signal, or use a hardware UART style receiver that samples at defined decision points. This insight informed the firmware approach: use framing, avoid relying on arbitrary software delays, and allow dedicated hardware or

comparator thresholding to provide cleaner digital transitions.

7.3 Serial Visibility and Debugging

A UART debug interface was used throughout development to print raw ADC readings, thresholded decisions, and received data. This visibility was essential for tuning thresholds under different ambient light conditions and for distinguishing analogue issues such as saturation or insufficient gain from digital issues such as timing and framing. After testing a software thresholding approach, the design moved toward using the PSoC comparator and UART hardware more effectively. The comparator created a clean logic signal, while the UART block could then handle start bit detection and sampling.

8 Experimental Methods

8.1 Bench Testing in Air

Initial testing was carried out in air to verify that the transmitter, receiver, and firmware operated correctly before introducing water. The transmitter LED output was checked visually and with an oscilloscope by monitoring the driver control waveform. The receiver output was observed at both the analogue amplifier stage and the comparator output stage. This allowed the raw photodiode/TIA signal to be compared directly with the restored digital comparator waveform.

The bench tests were used to confirm that the LED driver responded to the PSoC control signal, that the photodiode receiver produced a measurable response to optical pulses, and that the comparator could convert received analogue pulses into full swing digital transitions. These tests also revealed that direct UART decoding required the receiver waveform to reach a sufficiently high logic level, which limited communication range. This result led to the use of the IDAC comparator threshold method.

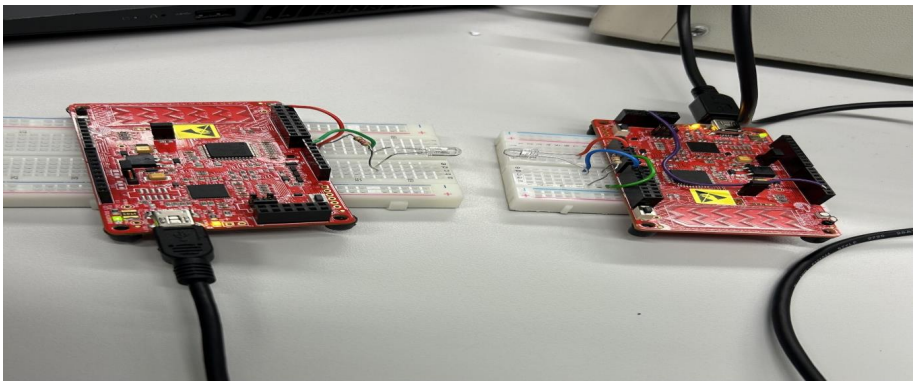

Figure 8.1: Bench air prototype.

8.2 Baud Rate and Bandwidth Testing

Baud rate testing was carried out to determine the practical speed limit of the communication link. The system was tested at several UART speeds while observing the transmitted and received waveforms on the oscilloscope. The receiver circuit was also modified by removing a redundant smoothing capacitor, which had been acting as an unwanted low pass filter. After removal, the received waveform had sharper edges and the usable detection rate improved significantly.

The TPS92612 LED driver was identified as the main speed limiting compo-

nent. Based on the rise and fall times from the datasheet, the practical modulation limit was expected to fall in the approximate range of 18.2–26.3 kbaud. This matched experimental observations, where 9600 baud was reliable but 19 200 baud produced inconsistent or corrupted data.

8.3 Waterproof Test Rig Method

A PVC pipe test rig was constructed to provide a defined optical path through water. The transmitter and receiver were mounted inside the pipe using a wooden alignment plank so that both ends remained fixed relative to each other. Waterproof enclosures were used to protect the electronics, with grommets, silicone sealing, O-rings, PTFE tape, and 3D printed supports used where required.

The test rig reduced ambient light and helped maintain alignment, but it also introduced internal reflections from the pipe wall. These reflections affected the received waveform at higher baud rates and contributed to intersymbol interference. For this reason, lower baud rates were used during successful underwater communication tests.

8.4 Underwater Communication Testing

Underwater testing was carried out using tap water, harbour water, and Ballybunion coastal water samples. The transmitter and receiver were placed inside the water filled test rig, and serial communication was monitored using a laptop. The baud rate, LED wavelength, LED current, supply arrangement, and comparator threshold were adjusted during testing.

The IDAC comparator threshold method was used as a practical way to compare received signal margin. The comparator reference was increased in small steps until the received optical signal could no longer reliably cross the threshold. A higher working IDAC baseline indicated a stronger received signal relative to the noise floor and background illumination.

8.5 Wavelength Comparison Method

The wavelength comparison used three LEDs: royal blue at approximately 448 nm, blue at approximately 475 nm, and green at approximately 530 nm. These wavelengths were selected because they cover the main blue green optical transmission window discussed in the theory chapter.

For each water sample, the same receiver threshold method was applied. The IDAC baseline was gradually increased until communication failed or be-

came intermittent. The maximum working threshold was recorded for each wavelength and used as an indicator of relative received signal strength. This method did not provide an absolute optical power measurement, but it provided a useful practical comparison between wavelengths under the same test conditions.

8.6 Recorded Metrics

The main recorded metrics were:

- Maximum working IDAC comparator baseline.
- Successful or failed serial data reception.
- Oscilloscope waveform shape and timing.
- Reliable and unreliable UART baud rates.
- Relative wavelength performance in different water samples.
- Practical mechanical and waterproofing issues observed during testing.

Future versions of the experiment should record additional quantitative data, including calibrated received voltage, noise level, SNR, BER, and optical power at the receiver.

9 Practical Development, Debugging and Field Results

9.1 Overview

The second phase of the project moved the UOWC link from a mainly theoretical and bench level design into a practical prototype. This included debugging the UART link, improving the receiver decision stage, increasing the usable signal bandwidth, refining the transmitter power system, constructing a controlled optical path, waterproofing the enclosure, and carrying out real water testing. The logbook evidence shows that the most important progress was not a single hardware change, but a sequence of electrical, firmware, and mechanical refinements that together made the underwater link work reliably enough for wavelength comparison.

A key lesson from this stage was that the system could not be treated as a simple digital UART cable replaced by light. The photodiode and TIA produced analogue pulses that were often visible on the oscilloscope even when the UART receiver could not decode them. This meant that the receiver required a proper decision stage between the analogue front end and the microcontroller. The project therefore shifted toward comparator based threshold detection using the PSoC IDAC as an adjustable baseline reference.

9.2 Updated LED Wavelengths and Transmitter Hardware

The practical wavelength set used in the final tests consisted of royal blue, blue, and green LEDs. These corresponded approximately to 448 nm, 475 nm, and 530 nm. The three wavelengths were chosen to cover the main blue green window discussed in the theory chapter, while also allowing the experiment to compare whether the tested water samples behaved more like clear ocean water, coastal water, or more turbid harbour water.

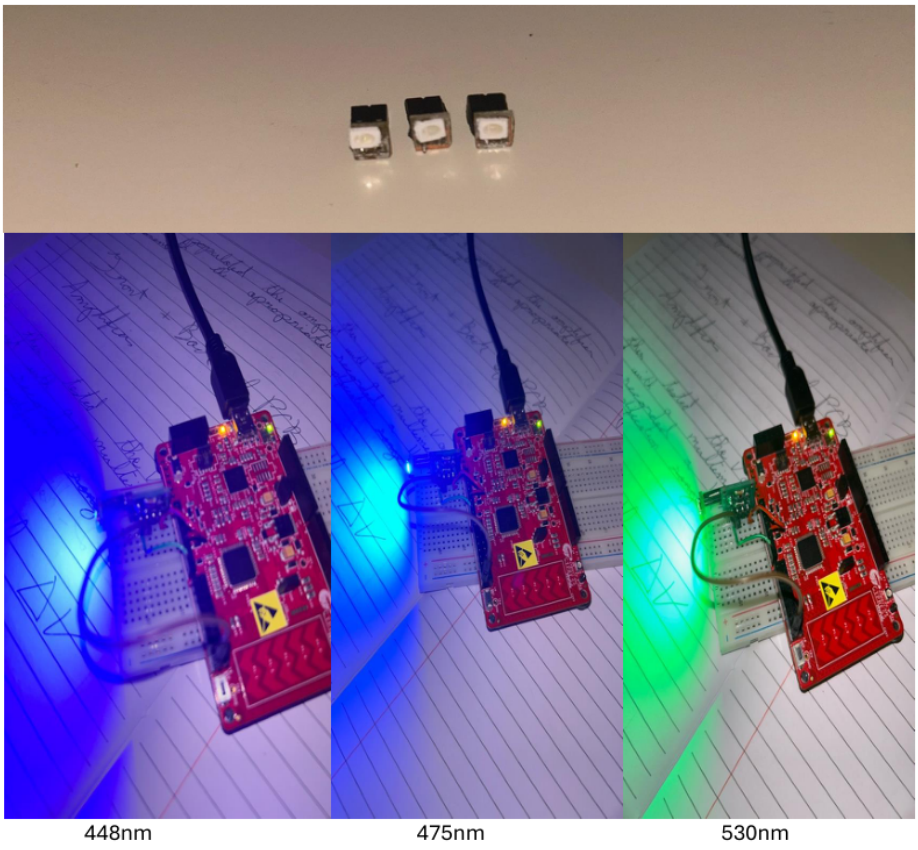

Figure 9.1: Practical LED wavelength set used for testing: royal blue 448 nm, blue 475 nm, and green 530 nm.

During early testing, the transmitter was not being driven as strongly as intended. Although the PSoC was powered from a 9 V battery, the LED driver was being supplied from the PSoC 3.3 V rail. This was not ideal for the TPS92612 driver, which performed better with a stable supply closer to 5 V. A new supply approach was therefore investigated using USB power banks capable of providing a 5 V output. This improved the transmitter supply arrangement and made it possible to target higher LED current in later tests.

The LED driver current setting resistor network was also modified to increase the LED drive current. The original effective sense resistance gave approximately 98 mA. By reducing the effective sense resistance, the target current was increased to roughly 140 mA. This change was made to increase optical power without redesigning the receiver amplifier, which was enclosed and more difficult to access without risk of damage. Increasing amplifier gain would have been a strong technical option, but the practical risk to the existing waterproof build made transmitter current increase the more suitable route.

9.3 UART Behaviour and Receiver Conditioning

Initial tests used a direct UART based optical link. This approach worked only when the optical signal drove the photodiode and TIA output fully into a valid digital logic level. In practice, this meant the received waveform had to rise close to the full logic swing and then return cleanly to baseline before the UART receiver could interpret it as a valid bit. This created an early range limitation of roughly below 0.4 m, even though weaker received pulses were still visible on the oscilloscope.

The UART transmitter also introduced a practical issue because a standard UART TX line idles high. Since the LED driver responded directly to the logic state, the LED could remain on when no useful data was being transmitted. This wasted power and shifted the optical baseline at the receiver. The preferred firmware approach is to allow the UART to finish transmitting, wait for the TX complete flag rather than relying on a fixed delay, and only then stop the UART or place the TX pin into a non driven High-Z state where suitable.

A separate communication fault was later traced to a missing common ground between the transmitter and receiver. When the transmitter was powered from a portable supply, the TX waveform initially appeared noisy. After correcting the oscilloscope grounding arrangement, the waveform itself was shown to be valid. The real fault was that the receiver had no shared reference for the transmitter signal. Once a common ground was added, normal UART communication returned. This was an important debugging result because it separated power supply concerns from the actual signal reference problem.

9.4 IDAC and Comparator Threshold Method

The main improvement in receiver operation came from using the PSoC comparator and IDAC as a programmable decision stage. The photodiode/TIA output was connected to the positive input of the comparator, while the IDAC generated a controllable reference level on the negative input. Any received optical pulse that exceeded this reference was converted into a full swing digital output. This allowed weaker analogue signals to be used, instead of requiring the raw receiver output itself to reach a UART logic threshold.

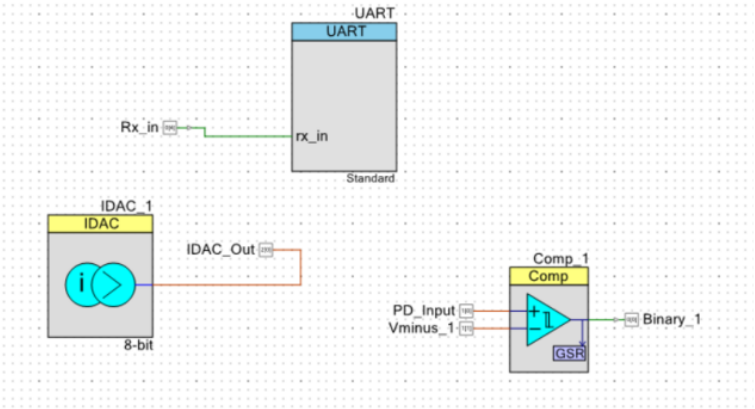

Figure 9.2: PSoC IDAC and comparator arrangement used to create an adjustable receiver threshold.

The comparator and IDAC method showed clear improvement during testing. By setting the threshold just above the noise floor, smaller received optical pulses could be converted into clean digital transitions. Oscilloscope comparison between the raw amplifier output and comparator output showed that the comparator restored the signal to a strong digital level even when the analogue pulse was relatively small.

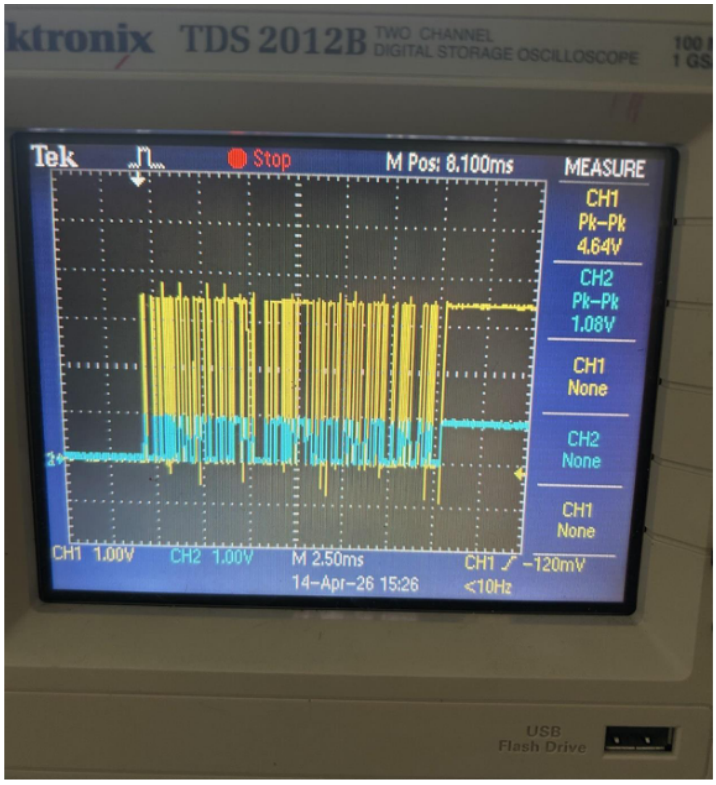

Previously, UART reception only worked when the analogue signal itself reached a full logic swing. With the comparator in place, smaller signals could still produce a valid logic output as long as they crossed the threshold.

Figure 9.3: Oscilloscope evidence of the comparator converting the smaller analogue receiver signal into a full-swing digital waveform.

This approach also introduced a useful future direction: software controlled auto-calibration. In a future version of the receiver, the IDAC could be adjusted automatically according to recent comparator history. If the comparator output stayed high for too long, the threshold could be raised; if it stayed low for too long, the threshold could be reduced. This would allow the receiver baseline to track slow changes in ambient light, alignment, or water conditions.

A second possible future improvement is an LDR based analogue compensation stage. An LDR in a voltage divider network could create a slow ambient dependent control voltage. As background illumination increases, the divider output would shift the photodiode/TIA operating point to reduce saturation risk. The photodiode and TIA would still detect the high speed optical signal, while the LDR would act only as a slow environmental compensation element. Initial tests with this concept appeared promising because the receiver behaved better under brighter conditions and showed less tendency toward saturation.

9.5 Bandwidth Investigation and Data Rate Limit

A redundant smoothing capacitor on the amplifier board was identified as a major bandwidth limitation. In this application the capacitor acted as an unwanted low pass filter, slowing the rise and fall times of the receiver waveform and rounding the edges of the digital signal. After the capacitor was removed, the receiver waveform became cleaner and the usable data rate improved significantly. The measured improvement was approximately an eight fold increase in practical detection rate.

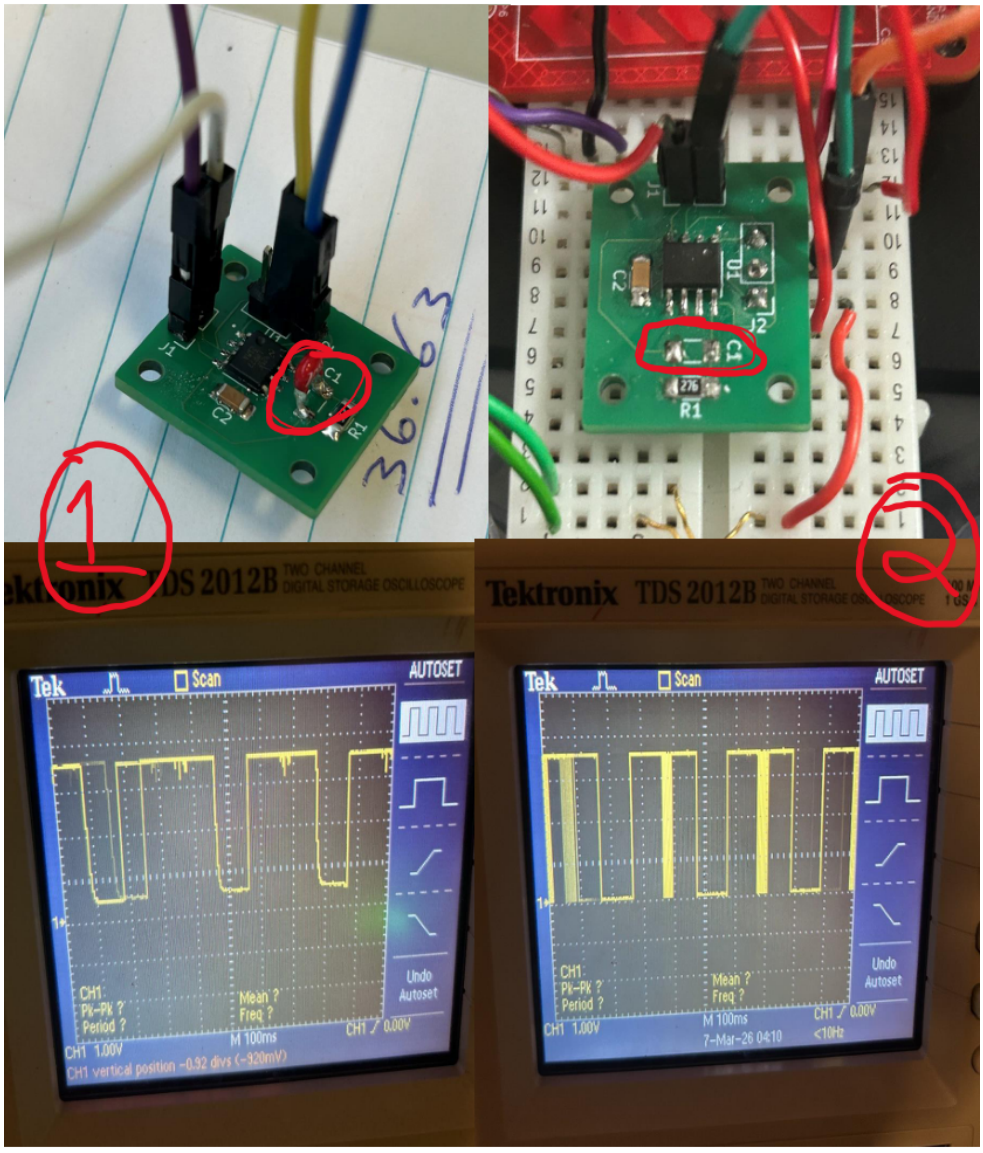

Figure 9.4: Receiver board and oscilloscope comparison before and after removal of the redundant smoothing capacitor.

Following this, the speed capability of the system was investigated. The PSoC UART and comparator were not expected to be the limiting factors, since

the comparator response is in the tens of nanoseconds and the UART can support the baud rates used in the project. Testing and datasheet review instead identified the TPS92612 LED driver as the main transmitter side speed bottle neck. Using the approximate switching period relation:

$$T_{\text{min}} \approx t_{\text{rise}} + t_{\text{fall}} \tag{9.1}$$

with typical values of approximately 17 µs rise time and 21 µs fall time gives:

$$f_{\text{max}} \approx \frac{1}{38\,\mu\text{s}} \approx 26.3\,\text{kHz} \tag{9.2}$$

Using slower worst-case switching values gives a maximum closer to 18.2 kHz. This range matched the practical results: 9600 baud was reliable, while 19 200 baud worked only inconsistently and produced shortened or corrupted received bit patterns.

Based on the drivers datasheet switching times of approximately **25 µs to 30 µs**, the theoretical maximum modulation rate was estimated to be in the region of **18.2 kbaud to 26.3 kbaud**. This aligned reasonably well with the observation that **19200 baud** only produced fully successful communication around **25% of the time**, indicating that operation at this rate was already near the practical limit. Below is a binary reading of Hello World! At 19200 baud, notice the binary is cut short in some cases.

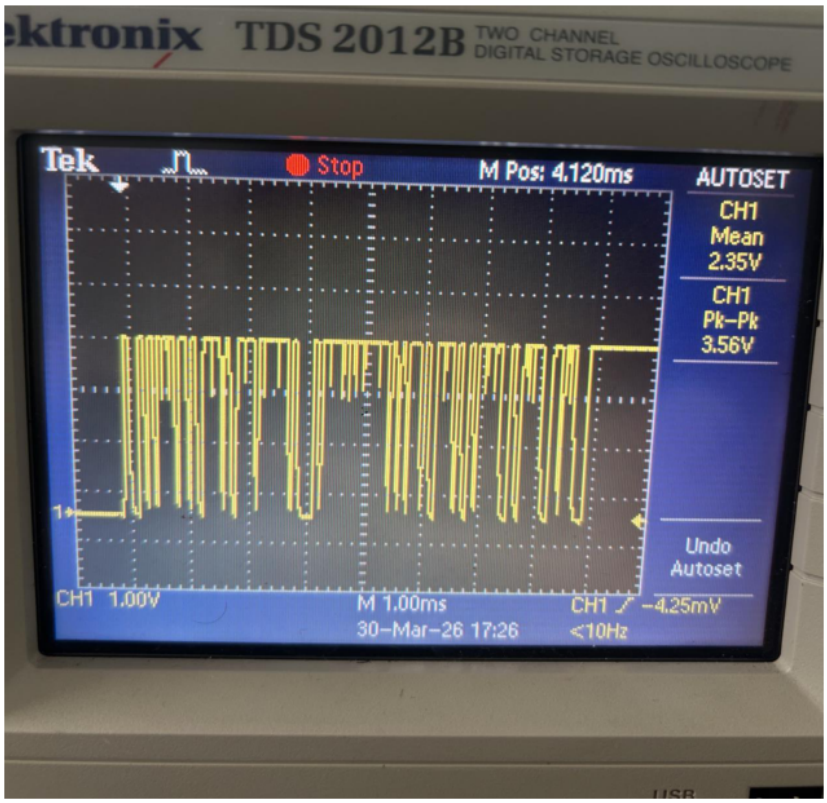

Figure 9.5: Oscilloscope trace from 19 200 baud testing, where the received binary pattern was inconsistent and sometimes cut short.

9.6 Mechanical Design and Waterproof Enclosure

A large part of the practical project involved turning the optical link into a repeatable and waterproof test assembly. Before the main pipe assembly was completed, the bottom of both micro controllers enclosures where found to be uneven because of protruding screw housings. A levelling insert was designed in Onshape using measurements taken with calipers and was printed on a Bambu Lab A1 Mini. This gave the case a flat, stable base and made later mounting and alignment work easier.

Figure 9.6: 3D printed base insert designed to level the enclosure and improve stability.

The main optical test structure was based on a PVC pipe, which provided a defined optical path and reduced the influence of ambient light. The pipe was cut to a manageable length and fitted with end caps. On the receiver side, a watertight enclosure was modified by drilling an opening for the receiver cable and fitting an electrical grommet. This cable allowed the receiver system to connect to a laptop for serial readout. The opening was heavily sealed with silicone, and the pipe cap arrangement used O-rings where possible to reduce leakage.

Figure 9.7: Receiver-side waterproofing arrangement with cable exit, grommet, sealing and pipe cap.

To maintain alignment, a wooden plank was installed along the inside of the pipe. This acted as the mounting structure for the transmitter and receiver, keeping both ends fixed relative to each other. The receiver electronics were mounted securely to the plank, while the transmitter side used a removable holder so that different LED wavelengths could be swapped during testing. The transmitter side was designed with a screw on cap so the LED source could be changed without rebuilding the full assembly.

Figure 9.8: Internal alignment plank and mounted transmitter/receiver electronics used to stabilise the optical path inside the PVC pipe.

Field handling revealed further mechanical issues. During the first beach water collection test, the transmitter side screw cap leaked slightly because a suitable O-ring was not available for the non standard thread. A custom silicone sealing ring was therefore considered, and later PTFE tape was identified as another practical improvement. The vertical handling of the pipe also created a risk of damaging the receiver-side cable and grommet. To solve this, a 3D printed stand was designed and made so that the tube could be supported vertically without loading the cable exit.

Figure 9.9: Final form of the UOWC system .

9.7 Successful Underwater Link and Multipath Behaviour

After the power supply and LED current improvements, underwater tests were repeated in tap water using all three LED wavelengths. During this phase, the UART baud rate was reduced on both the transmitter and receiver. This produced a major improvement and led to successful underwater optical communication through the test rig.

The improvement is likely linked to multipath reflections inside the reflec-

tive PVC pipe. The pipe creates delayed optical paths because light reflects from the internal surfaces before reaching the receiver. At lower baud rates, the symbol period is longer, so the receiver can make a correct decision before delayed reflected components have a major effect. At higher baud rates such as 2400 baud, 4800 baud, or 9600 baud in the reflective enclosure, the shorter symbol duration makes the system more sensitive to delayed reflections, causing intersymbol interference. This result showed that previous failures were not caused only by insufficient optical power; timing distortion from internal reflections also had a significant influence.

9.8 Wavelength Comparison Results

The final wavelength comparison used the IDAC controlled comparator threshold as a practical signal margin indicator. The IDAC baseline was increased in small steps until the received signal could no longer cross the comparator threshold. A higher stopping threshold indicated that the received signal had more margin above noise and background illumination.

In harbour water, the green LED stopped being detected when the comparator baseline reached approximately 6 mV. The royal blue LED continued until approximately 7.2 mV. This showed that, in the harbour water sample tested, royal blue produced a stronger received signal than green. This was somewhat unexpected because green light is often expected to perform better in dirtier or more turbid water. The result suggests that the harbour sample was not optically harsh enough for green to show a clear advantage, or that the attenuation profile during that test favoured the shorter wavelength.

Water sample	LED wavelength	Maximum working IDAC baseline
Harbour water	Green, approx. 530 nm	6.0 mV
Harbour water	Royal blue, approx. 448 nm	7.2 mV

Table 9.1: Harbour water wavelength comparison using the IDAC threshold method.

The coastal water tests produced better results overall. Green stopped being received at approximately 8.4 mV, blue at approximately 9.6 mV, and royal blue gave the strongest result, with occasional bits still detected at the upper test level. This suggests that the Ballybunion coastal water sample was relatively clear. Since Ballybunion is near the mouth of the Shannon Estuary, local freshwater mixing and coastal conditions may have influenced the optical properties of the sample. The result should therefore be treated as specific to the sampled conditions rather than a universal conclusion about all coastal water.

Water sample	LED wavelength	Maximum working IDAC baseline
Coastal water	Green, approx. 530 nm	8.4 mV
Coastal water	Blue, approx. 475 nm	9.6 mV
Coastal water	Royal blue, approx. 448 nm	9.6mV w/intermittent detection

Table 9.2: Coastal water wavelength comparison using the IDAC threshold method.

These results support the theory that the optimum wavelength depends on water type. However, they also show why practical measurement is necessary. Theoretical wavelength guidance based on Jerlov water types provides a useful starting point, but real water samples can vary with location, weather, suspended particles, organic matter, freshwater mixing, and collection method. For future work, oscilloscope monitoring should be added during field tests so that the raw analogue waveform, noise level, and threshold margin can be recorded alongside the USB serial output.

9.9 Evaluation of Practical Findings

The main practical finding is that the receiver decision method was more important than originally expected. The photodiode and amplifier were capable of detecting weaker optical pulses, but direct UART decoding wasted this information because the analogue pulse did not always meet the digital input requirements. The comparator and IDAC method solved this by separating analogue detection from digital logic recovery.

The second major finding is that the optical test enclosure influenced the communication channel. The PVC pipe improved ambient light rejection and alignment, but its reflective inner surface also introduced delayed optical paths. This produced a trade off: the enclosure made detection easier by reducing background light, while also making high speed UART decoding more vulnerable to intersymbol interference. This explains why reducing baud rate helped the system even after optical power was increased.

The third finding is that the system remained sensitive to mechanical robustness. Waterproofing, cable strain relief, cap sealing, case stability, and transport damage all affected testing reliability. The 3D printed base and stand, silicone sealing, grommet installation, and improved screw fixing were therefore not minor cosmetic improvements; they were necessary engineering changes that allowed repeatable testing.

10 Project Management

10.1 Timeline

The project spanned a 24 week development period. Figure 10.1, Figure **??**, and Figure **??** show the Gantt charts used to manage the project schedule across both semesters.

TASK	PROGRESS	START	END
Literature review/ research	80%	WEEK 1	WEEK 10
System Design	60%	WEEK 3	WEEK 12
Simulation and modelling	20%	WEEK 7	WEEK 10
Prototype and bench testing	15%	WEEK 8	WEEK 12
Water tank experiments and data collection	0%	WEEK 11	WEEK 12
Data analysis and Optimisation	0%	WEEK 12	WEEK 12
Final report and presentation	10%	WEEK 10	WEEK 12

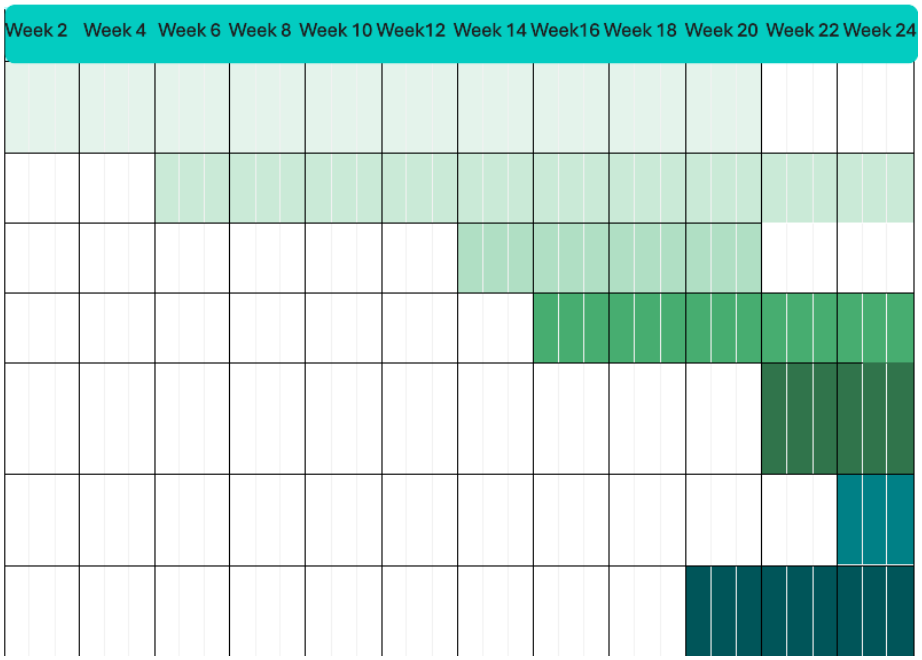

Figure 10.1: Gantt chart.

10.2 Risk Assessment

Risk	Impact	Mitigation
Poor optical alignment	Reduced received signal strength and increased communication errors.	Use a fixed internal mounting plank, controlled pipe geometry, and repeatable transmitter/receiver positioning.
High turbidity	Increased scattering and absorption, reducing range.	Test multiple water samples and compare wavelength performance using the IDAC threshold method.
Component failure	LED, driver, photodiode, or receiver hardware could fail during testing.	Use spare components where possible and test each subsystem before full integration.
Water ingress	Leakage could damage electronics and invalidate field tests.	Use grommets, silicone sealing, O-rings, PTFE tape, and careful leak checking before operation.
Ambient light interference	Background light could increase the noise floor or saturate the receiver.	Use a shielded pipe test rig, limited receiver field of view, and adjustable comparator thresholding.
Internal reflections	Reflections inside the PVC pipe could cause intersymbol interference.	Reduce baud rate and consider non-reflective internal lining in future work.
Time overrun	Mechanical fixes and debugging could reduce time available for final testing.	Use incremental testing and prioritise core communication functionality before optional improvements.

Table 10.1: Risk assessment and mitigation measures.

10.3 Safety, Ethics and Sustainability

Safety considerations included limiting LED current, avoiding unsafe optical exposure, protecting electronics from water ingress, and ensuring that power supplies were used correctly. The system used LEDs rather than lasers, reducing optical safety risk while still allowing useful underwater communication testing. Electrical safety was considered during battery, USB power bank, and bench supply use, particularly when testing near water.

The project did not involve human participants, animal subjects, or personal data. Ethical considerations were therefore limited to responsible testing, safe laboratory practice, and accurate reporting of results.

Sustainability considerations included reusing development boards, enclosures, cables, and optical components where possible. The design also supports future reuse because the transmitter, receiver, simulation code, and test rig can be modified rather than discarded. The use of low cost LEDs and reusable embedded hardware makes the prototype suitable for further educational development.

11 Discussion and Evaluation

The final prototype demonstrated that short range underwater optical communication can be achieved using low cost LEDs, a photodiode receiver, and PSoC based embedded hardware. The project also showed that the most difficult part of the system was not simply producing light underwater, but converting weak and noisy analogue optical pulses into reliable digital data.

The comparator and IDAC threshold method was the most important receiver improvement. Direct UART decoding required the raw receiver waveform to reach valid digital logic levels, which limited the link to very short distances. By introducing a programmable comparator threshold, smaller analogue pulses could be restored into full swing digital transitions. This improved the practical sensitivity of the receiver and provided a useful method for comparing wavelength performance.

The baud rate investigation showed that the system was limited mainly by the LED driver and analogue optical path rather than the PSoC UART itself. The TPS92612 switching time made 19 200 baud unreliable, while 9600 baud was more consistent under bench conditions. In the water filled pipe, lower baud rates were required because internal reflections produced delayed optical components and intersymbol interference.

The wavelength comparison results showed that royal blue and blue performed better than green in the tested harbour and coastal water samples. This agrees with the expectation that clearer water tends to favour shorter blue wavelengths, but the result should not be generalised too broadly. Real water quality changes with location, weather, suspended material, dissolved organic matter, and freshwater mixing. The Ballybunion coastal sample may have behaved closer to a clearer blue water condition, possibly influenced by local coastal conditions near the Shannon Estuary.

The mechanical build also had a major influence on the final outcome. Waterproofing, strain relief, cap sealing, enclosure stability, transport damage, and alignment all affected the reliability of testing. These practical issues showed that a UOWC system is not only an optical and electronic design problem, but also a mechanical integration problem.

11.1 Emerging Trends and Future Direction

Beyond the blue green LED, PIN/APD, and OOK/PPM link used in this project, current UOWC work is pushing in two directions: extreme data rates and much longer ranges. At the short to medium range end, blue lasers driven by OFDM variants combined with coding can sustain multi-gigabit transmission over controlled paths. At the long range end, recent work combines higher optical power, arrays of laser diodes, and advanced equalisation to extend UOWC performance to much longer distances in tank demonstrations.

Researchers are also engineering the spatial structure of the link to make laser based systems less fragile. One approach applies MIMO ideas using multiple transmit and receive apertures to create partially independent spatial paths, reducing sensitivity to bubbles, misalignment, and fading. Another approach shapes the beam using metasurfaces that sculpt the outgoing wavefront into Airy beams that can self accelerate and self heal, improving link stability in perturbed water channels. Image based tracking and feedback control can further help maintain alignment between narrow beams and moving receivers. These approaches are beyond the scope of the present prototype but provide useful direction for future research.

12 Conclusion and Future Work

This project successfully designed, built, and tested a low cost underwater optical wireless communication prototype using visible LEDs, a photodiode receiver, analogue signal conditioning, comparator threshold detection, and PSoC embedded hardware. The system demonstrated underwater optical communication through a water filled test assembly and provided practical wavelength comparison results for royal blue, blue, and green LEDs.

The project began with the theory of UOWC, where acoustic and RF underwater communication limitations were used to justify the use of visible optical links for short range, low latency, higher data rate applications. The blue green transmission window was identified as the most suitable wavelength region, leading to the selection of LEDs at approximately 448 nm, 475 nm, and 530 nm. A literature review informed the choice of IM/DD communication, OOK style signalling, photodiode detection, optical filtering, and Beer Lambert based modelling.

A major practical finding was that direct UART decoding was not suitable for weak received optical signals. The photodiode and TIA could produce visible analogue pulses, but these pulses were often too small or too noisy to be interpreted directly as digital UART levels. The use of the PSoC comparator and IDAC solved this issue by creating an adjustable receiver threshold. This allowed smaller analogue signals to be converted into full swing digital outputs and significantly improved the usefulness of the receiver.

The project also identified several important limitations. The TPS92612 LED driver limited the practical data rate because of its switching response, with 9600 baud reliable under suitable conditions and 19 200 baud close to the practical limit. The PVC pipe test rig improved alignment and reduced ambient light but introduced internal reflections that caused intersymbol interference at higher baud rates. Mechanical issues such as sealing, cable strain relief, enclosure stability, and transport damage also affected testing and required practical design improvements.

The final wavelength comparison showed that royal blue and blue performed better than green in the tested harbour and Ballybunion coastal water samples. In harbour water, green stopped working at approximately 6.0 mV IDAC baseline, while royal blue continued to approximately 7.2 mV. In coastal water, green reached approximately 8.4 mV, blue reached approximately 9.6 mV, and royal blue gave the strongest overall result with intermittent detection at the final threshold step. These results suggest that the tested coastal sample

was relatively clear and that practical wavelength selection should be based on measured water conditions rather than theory alone.

Future work should focus on improving optical alignment, reducing internal reflections, increasing receiver sensitivity, and collecting more quantitative measurements. The inside of the PVC pipe could be made less reflective to reduce multipath effects. The receiver could be redesigned with a lower noise TIA, better shielding, and a more stable comparator threshold circuit. A calibrated optical power or voltage measurement should be recorded during each test so that SNR and BER can be calculated more accurately. The Python simulation should also be calibrated using measured data so that it can predict received voltage and communication range more realistically.

Further improvements could include automatic IDAC threshold calibration, LDR based ambient light compensation, optical bandpass filters, improved lenses, APD receiver testing, packet framing with CRC error detection, and more advanced modulation such as PPM. With these improvements, the prototype could develop from a proof of concept communication link into a more robust underwater optical modem platform.

References

Engineered Science (2021) ‘Underwater optical communication: A comprehensive review’. *Engineered Science*, 9(2), pp. 97–104. Available at: https://www.espublisher.com/journals/articledetails/574 (Accessed: 21 November 2025).

GeeksforGeeks (2020) ‘Pulse position modulation (PPM) and pulse width modulation (PWM)’. Available at: https://www.geeksforgeeks.org/ (Accessed: 29 November 2025).

Hamamatsu Photonics (2020) *S12053 series silicon avalanche photodiodes* (datasheet). Available at: https://www.hamamatsu.com (Accessed: 1 December 2025).

Hamamatsu Photonics (2025) *S5345 Si APD short wavelength type* (datasheet). Available at: https://www.hamamatsu.com (Accessed: 21 November 2025).

Hamamatsu Photonics (n.d.) *S5973-02 silicon photodiode* (datasheet). Available at: https://www.hamamatsu.com (Accessed: 9 November 2025).

Hamamatsu Photonics (n.d.) *Guide to detector selection*. Hamamatsu Photonics Knowledge Hub. Available at: https://hub.hamamatsu.com/us/en/technical-notes/detector-selection/guide-to-detector-selection.html (Accessed: 10 December 2025).

Kaushal, H. and Kaddoum, G. (2016) ‘Underwater optical wireless communication’, *IEEE Access*, 4, pp. 1518–1547. Available at: https://ieeexplore.ieee.org/stamp/stamp.jsp?tp=&arnumber=7450595 (Accessed: 12 November 2025).

Lumileds (n.d.) *LUXEON 3535L Color Line* (datasheet). Available at: https://www.lumileds.com/ (Accessed: 20 November 2025).

Pope, R.M. and Fry, E.S. (1997) ‘Absorption spectrum (380–700 nm) of pure water. II. Integrating cavity measurements’, *Applied Optics*, 36(33), pp. 8710–8723.

Schirripa Spagnolo, G., Cozzella, L. and Leccese, F. (2020) ‘Underwater Optical Wireless Communications: Overview’, *Sensors*, 20(8), 2261. Available at: https://doi.org/10.3390/s20082261 (Accessed: 10 November 2025).

Schirripa Spagnolo, G. et al. (2025) ‘LEDs for Underwater Optical Wireless Communication’, *Photonics*, 12(8), 749. (Accessed: 22 November 2025).

Texas Instruments (2020) *TPS92612-Q1 automotive single channel LED driver* (datasheet). Available at: https://www.ti.com/ (Accessed: 21 November 2025).

Weiskerger, C.J. et al. (2018) 'Application of the Beer Lambert Model to Attenuation of Underwater Light', *Water Resources Research*, 54(8), pp. 5715–5730. Available at: https://repository.library.noaa.gov/view/noaa/20744 (Accessed: 9 November 2025).

Zayed, M.M. and Shokair, M. (2025a) 'Performance analysis and optimization of modulation techniques for underwater optical wireless communication in varied aquatic environments', *Scientific Reports*, 15, Article 32570. (Accessed: 10 November 2025).

Zayed, M.M. and Shokair, M. (2025b) 'Modeling and simulation of optical wireless communication channels in IoUT considering water types, turbulence and transmitter selection', *Scientific Reports*, 15, Article 28381. Available at: https://pmc.ncbi.nlm.nih.gov/articles/PMC12322103/ (Accessed: 12 November 2025).

Zhang, M. et al. (2023) 'Real Time Underwater Wireless Optical Communication with Blue LEDs', *Sensors*, 23(15), 6753. (Accessed: 12 November 2025).

Oubei, H.M. et al. (2015) '4.8 Gbit/s 16-QAM-OFDM transmission based on compact 450-nm laser for underwater wireless optical communication', *Optics Express*, 23(18), pp. 23302–23309.

Hu, J., Guo, Z., Shi, J. et al. (2024) 'A metasurface-based full-color circular auto-focusing Airy beam transmitter for stable high-speed underwater wireless optical communications', *Nature Communications*, 15, 2944. Available at: https://doi.org/10.1038/s41467-024-47105-x (Accessed: 11 December 2025).

Chen, Z., Liu, Y., Yi, X. and Zhao, R. (2025) 'Angular Circle Array Multiple Input Multiple Output Underwater Optical Wireless Communications', *Photonics*, 12, 12. Available at: https://doi.org/10.3390/photonics12010012 (Accessed: 8 December 2025).

A Example Calculation

This appendix gives a simple feasibility template aligned with the project link budget model. Given transmitted optical power P_t, distance d, attenuation coefficient $c = \alpha + \beta$, and an overall coupling or efficiency factor η that lumps transmitter/receiver optics and alignment, the received optical power is estimated by:

$$P_r = P_t \eta e^{-cd} \tag{A.1}$$

For an LED source, η implicitly includes Lambertian emission and geometric collection, including finite receiver area, divergence, and field of view effects. For a laser source it similarly represents divergence limited spreading and collection. The received optical power is converted to photodiode current using the detector responsivity:

$$I_p = R(\lambda) P_r \tag{A.2}$$

Feasibility is then assessed by comparing I_p against the receiver noise and threshold margin, including shot noise, thermal noise, dark current noise, and any additional receiver specific noise terms. In practice, η aggregates lens transmission, filter transmission, geometric collection efficiency, and alignment. It can be calibrated by measuring received photocurrent or voltage at known distances and fitting η and an effective c to the measured decay.

B Firmware Excerpt

The following excerpt illustrates the UART based ADC readout and thresholding used during early debugging. This code was useful for observing receiver behaviour during development, but the final system moved toward comparator based threshold detection because direct ADC thresholding was too sensitive to timing drift and weak analogue signal levels.

Listing B.1: Firmware excerpt used during early debugging

```
#include "project.h"
#include <stdio.h>
#include <math.h>

// Constants
#define LED1_Channel    0
#define TAB             0x09

int binary_out;

// Variable declarations
char str[32];
char byte_str[32];
char choice = 100;

uint8 I = 0;
uint16 Calculated_Tx_Rate;
uint16 PD_Number;          // Photodiode ADC Number
uint16 Ambiant_Light = 800;

// New variables for assembling bits into a byte
uint8 bit_index = 0;
uint8 rx_byte   = 0;

int main(void)
{
    CyGlobalIntEnable; /* Enable global interrupts. */

    ADC_Start();
    UART_Start();
    PWM_LED1_Start();
```

```
UART_PutString("\x1b[2J\x1b[;H");
UART_PutCRLF(TAB);
UART_PutCRLF(TAB);
UART_PutString("LED Photodiode Test");
UART_PutCRLF(TAB);
CyDelay(700);

for(;;)
{
    ADC_StartConvert();
    ADC_IsEndConversion(ADC_WAIT_FOR_RESULT);
    PD_Number = ADC_GetResult16(LED1_Channel);

    sprintf(str, "%d", PD_Number);
    UART_PutString(" Photodiode Reading = ");
    UART_PutString(str);

    if (PD_Number > Ambiant_Light)
    {
        binary_out = 1;
    }
    else
    {
        binary_out = 0;
    }

    sprintf(str, "%d", binary_out);
    UART_PutString(", Binary Reading = ");
    UART_PutString(str);
    UART_PutCRLF(TAB);

    if (binary_out)
    {
        rx_byte |= (1u << bit_index);   // LSB first
    }

    bit_index++;

    if (bit_index >= 8u)
    {
```

```
            sprintf(byte_str, "Received Byte = 0x%02X (%u)", rx_byte,
    rx_byte);
            UART_PutString(byte_str);
            UART_PutCRLF(TAB);

            bit_index = 0u;
            rx_byte   = 0u;
        }
    }
}

/* [] END OF FILE */
```

C UART Transmitter Firmware Excerpt

The following firmware excerpt shows the final UART transmitter structure used to send a framed message through the optical link. Each transmission begins with the header `Tx:`, followed by a number that cycles from 1 to 100, and ends with the tail `UOWC`. This framing method made it easier for the receiver firmware to check whether the detected message was valid, rather than only reacting to random received characters or noise.

The use of the UART transmit done flag also improved the timing of the transmitter code. Instead of relying only on a fixed delay after sending data, the firmware waits until the UART hardware confirms that the full message has finished transmitting before continuing. This helps avoid stopping or changing the transmitter state before the last byte has fully left the UART buffer.

Listing C.1: UART transmitter firmware using header, payload number and tail

```
#include "project.h"
#include <stdio.h>

int main(void)
{
    CyGlobalIntEnable;

    uint8_t txNumber = 1u;
    char txBuffer[32];

    UART_Start();

    for(;;)
    {
        UART_ClearTxInterruptSource(UART_INTR_TX_UART_DONE);

        sprintf(txBuffer, "Tx: %u UOWC.\r\n", txNumber);
        UART_UartPutString(txBuffer);

        while ((UART_GetTxInterruptSource() & UART_INTR_TX_UART_DONE) ==
    0u)
        {
        }

        UART_ClearTxInterruptSource(UART_INTR_TX_UART_DONE);
```

```
            txNumber++;
            if (txNumber > 100u)
            {
                txNumber = 1u;
            }

            CyDelay(2000);
        }
    }
```

D UART Receiver Firmware Excerpt

The following receiver firmware was used on the separate PSoC receiver module. The IDAC and comparator are started first so that the analogue photodiode signal can be converted into a digital logic signal for the UART input. The received UART message is stored until the end of the line is detected. The firmware then checks that the message begins with the header `Tx:`, ignores the number in the middle, and confirms that the message ends with the tail `UOWC.`. If the expected structure is not detected, the receiver outputs `communication error`.

Listing D.1: UART receiver firmware checking header and tail

```
#include <project.h>
#include <stdio.h>

#define RX_BUFFER_SIZE 32u

char rxBuffer[RX_BUFFER_SIZE];
uint8 rxIndex = 0u;

uint8 CheckFrame(char *buffer)
{
    uint8 i = 0u;

    if (buffer[0] != 'T') return 0u;
    if (buffer[1] != 'x') return 0u;
    if (buffer[2] != ':') return 0u;
    if (buffer[3] != ' ') return 0u;

    i = 4u;

    if (buffer[i] < '0' || buffer[i] > '9')
    {
        return 0u;
    }

    while (buffer[i] >= '0' && buffer[i] <= '9')
    {
        i++;
    }
```

```
    if (buffer[i] != ' ') return 0u;
    i++;

    if (buffer[i] != 'U') return 0u;
    if (buffer[i + 1u] != 'O') return 0u;
    if (buffer[i + 2u] != 'W') return 0u;
    if (buffer[i + 3u] != 'C') return 0u;
    if (buffer[i + 4u] != '.') return 0u;
    if (buffer[i + 5u] != '\0') return 0u;

    return 1u;
}

int main(void)
{
    CyGlobalIntEnable;

    IDAC_1_Start();
    Comp_1_Start();
    UART_Start();

    UART_UartPutString("Receiver started\r\n");

    for(;;)
    {
        uint32 ch = UART_UartGetChar();

        if (ch != 0u)
        {
            if (ch == '\r')
            {
            }
            else if (ch == '\n')
            {
                rxBuffer[rxIndex] = '\0';

                if (CheckFrame(rxBuffer))
                {
                    UART_UartPutString("Valid message received: ");
                    UART_UartPutString(rxBuffer);
```

```
                    UART_UartPutString("\r\n");
                }
                else
                {
                    UART_UartPutString("communication error\r\n");
                }

                rxIndex = 0u;
            }
            else
            {
                if (rxIndex < (RX_BUFFER_SIZE - 1u))
                {
                    rxBuffer[rxIndex] = (char)ch;
                    rxIndex++;
                }
                else
                {
                    rxIndex = 0u;
                    UART_UartPutString("communication error\r\n");
                }
            }
        }
    }
}
```

E GitHub Link for Python Simulation

https://github.com/EmilBH112/UOWC_Attenuation_Model.git